SPECIAL ISSUE ARTICLE



Check for updates



Nasopharyngeal morphology contributes to understanding the "muddle in the middle" of the Pleistocene hominin fossil record

Anthony S. Pagano¹ | Christopher M. Smith^{2,3,4} | Antoine Balzeau⁵ | Samuel Márquez⁶ | Jeffrey T. Laitman^{2,3,4} |

Correspondence

Anthony S. Pagano, Department of Medical Sciences, Hackensack Meridian School of Medicine, 4400 Suite, 123 Metro Blvd, Nutley, NJ 07110, USA. Email: anthony.pagano@hmhn.org

Funding information

This work was assisted by a grant from the National Science Foundation (Grant number 1128901)

Abstract

The late archeologist Glynn Isaac first applied the term "muddle in the middle" to a poorly understood period in the Middle Pleistocene human fossil record. This study uses the nasopharyngeal boundaries as a source of traits that may inform this unclear period of human evolution. The nasopharynx lies at the nexus of several vital physiological systems, yet relatively little is known about its importance in human evolution. We analyzed a geographically diverse contemporary *Homo sapiens* growth series (n = 180 adults, 237 nonadults), Homo neanderthalensis (La Chapelle aux Saints 1, La Ferrassie 1, Forbes Quarry 1, Monte Circeo 1, and Saccopastore 1), mid-Pleistocene Homo (Atapuerca 5, Kabwe 1, Petralona 1, and Steinheim 1), and two Homo erectus sensu lato (KNM-ER 3733 and Sangiran 17). Methods include traditional (Analysis 1) and 3D geometric morphometric analysis (Analysis 2). H. erectus exhibited tall, narrow nasopharyngeal shape, a robust, ancestral morphology. Kabwe 1 and Petralona 1 plotted among H. sapiens in Analysis 2, exhibiting relatively shorter and vertical cartilaginous Eustachian tubes and vertical medial pterygoid plates. Atapuerca 5 and Steinheim 1 exhibited horizontal vomeral orientation similar to H. neanderthalensis, indicating greater relative soft palate length and anteroposterior nasopharynx expansion. They may exhibit synapomorphies with H. neanderthalensis, supporting the accretionary hypothesis. Specieslevel differences were found among H. sapiens and H. neanderthalensis, including relatively longer dilator tubae muscles and extreme facial airorhynchy among Neanderthals. Furthermore, H. neanderthalensis were autapomorphic in exhibiting horizontal pterygoid plate orientation similar to human infants, suggesting that they may have had inferiorly low placement of the torus tubarius and Eustachian tube orifice on the lateral nasopharyngeal wall in life. This study supports use of osseous nasopharyngeal boundaries both for morphological characters and understanding evolution of otitis media susceptibility in living humans.

¹Department of Medical Sciences, Hackensack Meridian School of Medicine, Nutley, New Jersey, USA

²Department of Anthropology, CUNY Graduate Center, New York, New York, USA

³New York Consortium in Evolutionary Primatology, New York, New York, USA

⁴Center for Anatomy and Functional Morphology, Icahn School of Medicine, New York, New York, USA

⁵Department de Homme et environnement, Musée de l'Homme— Palais de Chaillot, Paris, France

⁶Departments of Cell Biology and Otolaryngology, SUNY Downstate Health Sciences University, Brooklyn, New York, USA

1 | INTRODUCTION

The nasopharynx is a region lying at the intersection of the nasal cavity, oral cavity, basicranium, and middle ear. Largescale changes have occurred among its boundaries (Figure 1) over the course of human evolution (e.g., Bastir, 2019; Bastir & Rosas, 2016; Dean & Wood, 1982; Laitman & Heimbuch, 1982; Pagano et al., 2019; Spoor, 1997) related to facial orthognathy, basicranial flexion, and coronal orientation of the petrous temporal bones acting to reduce the anteroposterior length of the airway while increasing its mediolateral width (Dean, 1982). These changes relate functionally to a reconfiguration of the upper airway that has rendered Homo sapiens the only known living species to exhibit a two-tubed aerodigestive tract in which the soft palate and epiglottis lose contact over early postnatal development (e.g., Laitman & Reidenberg, 2009; Negus, 1949). Simultaneously, growth change in these structures likely underlies the reason our species suffers uniquely and endemically from chronic otitis media and rhinosinusitis as the upper airways of infants and young children are inefficient at equilibrating middle ear pressure and clearing the middle ear cavity and paranasal sinuses (Bluestone, 2005; Bluestone et al., 2012; Pagano et al., 2017, 2021).

Evolutionary changes in nasopharyngeal structures are of interest both within the context of the evolution of human disease and as sources of morphological characters whose phylogenetic polarity among fossil humans is not yet understood. To this end, we undertook analysis of the osseous nasopharyngeal boundaries (Figure 2) among a geographically diverse sample of contemporary humans (used here to represent H. sapiens), Neanderthals (i.e., specimens that have been assigned previously to Homo neanderthalensis; e.g., Tattersall & Schwartz, 1998), European and African mid-Pleistocene Homo (mPH; specimens traditionally assigned to Homo heidelbergensis, e.g., Stringer, 1983), and Homo erectus sensu lato (including specimens assigned to both Homo ergaster such as KNM-ER 3733 and Homo erectus such as Sangiran 17; hereafter referred to as H. erectus). We opted for the term mPH as it is interchangeable with H. heidelbergensis (sensu Stringer, 1983) while accounting simultaneously for the nonmonophyletic nature of this group (see below). It was our goal to allow nasopharyngeal morphology to sort these specimens rather than juxtaposing observed morphological variation over previously assigned taxonomic rankings.

This study follows work by Pagano et al. (2019) identifying potential species-level differences between *H. sapiens* and *H. neanderthalensis*, particularly in the horizontal orientations of the choanae and cartilaginous Eustachian (pharyngotympanic) tubes (CETs) in the former group relative to the latter. Here, we reconstruct the origins of the

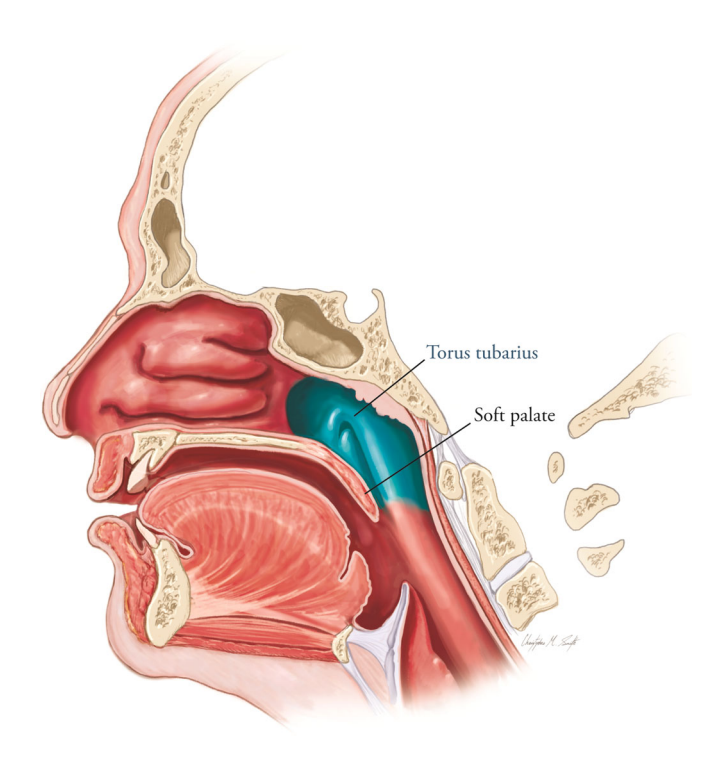


FIGURE 1 Parasagittal section of a human head. Nasopharyngeal boundaries are highlighted in blue

H. sapiens and *H. neanderthalensis* conditions via comparison to geologically older specimens of mid-Pleistocene age, analyzing the functional and evolutionary implications of their nasopharyngeal morphology.

1.1 | The "muddle in the middle" and defining mid-Pleistocene hominin taxa

The term "muddle in the middle" was applied initially by Isaac (1975) to this Middle Pleistocene period, spanning between the Brunhes-Matuyama paleomagnetic boundary (approximately 780 ka) and the end of the penultimate glaciation event (approximately 130 ka). He discussed discrepancies in the paleoclimatology, dating, and archaeology within this time. The taxonomic affinities of many Middle Pleistocene fossil specimens are also unclear. Workers have described specimens of Middle Pleistocene age as archaic H. sapiens. The term archaic H. sapiens was first introduced by Mayr (1950) and then refined by Howells (1980) to describe these fossil specimens as exhibiting both sapiensand erectus-like traits but with brain size larger than the latter group. Others used this term to describe specimens that were believed at the time to represent populations that graded anagenetically (or evolved gradually) into H. sapiens while exhibiting cranial capacity greater than 1,200 cc (Santa Luca, Santa, 1978; Stringer et al., 1979). However, untenability of this term was discussed by

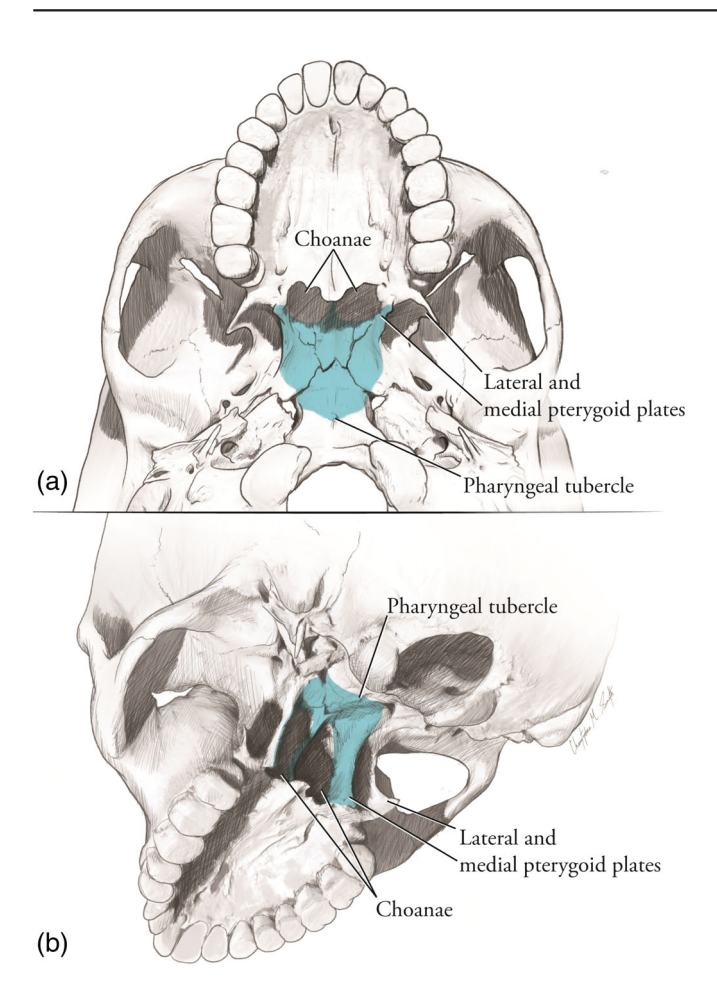


FIGURE 2 Osseous nasopharyngeal boundaries in in blue from (a) basal and (b) oblique posterior view. These include the choanal boundaries, basisphenoid, and basiocciput

Tattersall (1986) who noted that many living humans do not cross the "cerebral Rubicon" of 1,200 ml brain size delimiting archaic H. sapiens (see extensive review by 2007). The species designation H. heidelbergensis came to replace the nontaxonomic title of archaic H. sapiens and included specimens that are not grouped relative to their shared derived traits but instead by exclusion from other species (contra Hennigian cladistics; Hennig, 1966). This species name was first applied to the Mauer 1 mandible from Germany (the holotype or specimen upon which the species is defined) by Schoetensack (1908). Stringer (1983) later included into this group all specimens post-dating H. erectus but predating the appearance of H. sapiens and H. neanderthalensis. With the stated aim of describing the common ancestor of H. sapiens from Africa and H. neanderthalensis from Europe and Western Asia, the species designation of H. heidelbergensis was applied to specimens spanning all three continents. While some have supported Stringer's (1983) usage of H. heidelbergensis (e.g., Bräuer, 2008; Mounier & Lahr, 2016; Rightmire, 1998) others have posited instead the existence of multiple species

as there is a great amount of morphological diversity among the members of this group (e.g., Hublin, 2009; Martinón-Torres et al., 2012; Stringer, 2012). Sima de los Huesos fossils, for example, express derived H. neanderthalensis traits to the exclusion of other specimens in Europe and Africa, leading some to place them instead within H. neanderthalensis (Arsuaga et al., 1997, 2014; Bermúdez de Castro et al., 2019; Stringer, 2012). Furthermore, specimens such as Petralona 1 from Greece and Zuttiyeh 1 from Israel exhibit ambiguous patterns of morphology (e.g., Freidline et al., 2012; Roksandic et al., 2018), raising the possibility that their populations were not directly ancestral to H. neanderthalensis. It was proposed instead that there were multiple populations within Europe and Western Asia at this time (Arsuaga et al., 2014; Hanegraef et al., 2018; Stringer, 2012) with the Iberian Peninsula acting as a glacial refugium or southern European zone to which hominin populations withdrew during periods of extreme cold in the rest of the continent. It was here that the ancestors of H. neanderthalensis may have arisen in geographical isolation relative to other locations, being limited initially by the Pyrenees mountains. The Balkan peninsula, in contrast, was well connected to Western Asia throughout the Middle Pleistocene (Roksandic et al., 2018). In areas outside of Iberia, "Neanderthalization" would not have occurred as geneflow maintained more primitive morphology among these interconnected populations (Roksandic et al., 2018). The designation of H. heidelbergensis would thus be reserved for both specimens that are older than the Sima de los Huesos fossils (approximately 455 ka; Demuro et al., 2019) and sufficiently ancestral to exhibit no H. neanderthalensis or H. sapiens traits (Arsuaga et al., 2014) and for later specimens such as Petralona 1 that maintain this primitive cranial morphology outside of Western Europe (Roksandic et al., 2018). Under such a definition, H. heidelbergensis could still be considered a species ancestral to both H. sapiens and H. neanderthalensis with Mauer 1 remaining an appropriate holotype as it is relatively old (approximately 609 ka; Wagner et al., 2010) and appears to lack H. neanderthalensis traits (Martinón-Torres & Bermúdez de Castro, 2015; Skinner et al., 2016).

There has been much debate surrounding the taxonomic status of fossils subsumed within mPH with still no clear consensus (see above). Rather than representing a well-defined taxonomic group, the mPH sample used here is instead a temporal group meant to represent a collection of specimens that could, as a function of their age, maintain some aspects of nasopharyngeal morphology that are ancestral relative to *H. sapiens* and *H. neanderthalensis*. The term "mid-Pleistocene *Homo*" (Athreya, 2007; Wang, 2011; Xiao et al., 2014) was preferred over *H. heidelbergensis* as the former is not a taxonomic name. It was also chosen for the

purpose of excluding *H. sapiens* of late Middle Pleistocene age such as those from Omo Kibish (Day, 1969), Herto (White et al., 2003), and Jebel Irhoud (Hublin et al., 2017). A similar naming controversy has surrounded the use of *H. erectus*, in which its great temporal and geographic ranges have led to long-standing controversies over whether one or more species are contained within this group (see Baab, 2008 for a detailed review). This topic is beyond the scope of the current study and we opted to use "*H. erectus sensu lato*." Our aim was to identify nasopharyngeal morphology that is ancestral relative to *H. sapiens* and *H. neanderthalensis* by describing one African (KNM-ER-3733) and one South East Asian (Sangiran 17) *H. erectus* cranium.

Our aim here is to ascertain the polarity of traits among mPH specimens using H. sapiens and H. neanderthalensis as crown species. Among the most widely used definitions of crown taxa is by De Quieroz and Gauthier (1992) as: "groups that stem from the most recent common ancestor of sister taxa with extant representatives." We treat H. neanderthalensis as a crown species for the narrow purpose of the analysis as they became extinct only recently and represent the endpoint of a parallel evolutionary lineage to that of living H. sapiens. We also use one African (KNM-ER3733) and one South East Asian (Sangiran 17) specimen attributed to H. erectus sensu lato both as out groups and as representatives of broadly ancestral morphology relative to later hominins despite their geographical and temporal distance from each other. Moreover, we analyze the morphology of Atapuerca 5, Kabwe 1, Petralona 1, and Steinheim 1 to identify phylogenetically important patterns of variation that may suggest either relatedness to one of the crown groups or retention of ancestral morphology if found to be similar to H. erectus sensu lato.

1.2 | Hypotheses

Hypothesis 1. The Western European mPH specimens (Atapuerca 5 and Steinheim) express derived nasopharyngeal morphology in common with *H. neanderthalensis* relative to *H. sapiens* and mPH outside of this region (Kabwe 1, Petralona 1).

The accretionary hypothesis posits that *H. neanderthalensis* originated from a group of European mPH that exhibited *H. neanderthalensis* traits, such as the specimens from the Middle Pleistocene Sima de los Huesos site (e.g., Arsuaga et al., 1997, 2014; Dean et al., 1998; Hublin, 2009). Some shared derived morphology may also lie among the osseous nasopharyngeal boundaries, excluding by definition either specimen from *H. heidelbergensis*

(as per Arsuaga et al., 2014; see above). To test Hypothesis 1, we examined whether Atapuerca 5 and Steinheim 1 exhibited any shared derived aspects of osseous nasopharyngeal morphology with Neanderthals.

Hypothesis 1 would be accepted if either the Atapuerca 5 or Steinheim 1 cranium clustered with *H. neanderthalensis* in a Principal Components Analysis of overall nasopharyngeal shape to the exclusion of *H. sapiens* and mPH from outside Western Europe or if values for univariate measures of choanal, CET, or dilator tubae muscle morphology were similar among the two groups to the exclusion of other fossils.

Hypothesis 2. Kabwe 1 and Petralona 1 share derived aspects of nasopharyngeal morphology with *H. sapiens* to the exclusion of *H. neanderthalensis* and Western European mP*H*.

The geological age of the Kabwe 1 cranium has been estimated to be as old as 500-700 ka using faunal data (Avery, 2002) while Grün et al. (2020) have provided a much younger age of approximately 300 ka using radiometric methods. If the older date were correct, Kabwe 1 could be considered among several African mPH specimens, including Bodo 1, Ndutu 1, and Eliye Springs 1. However, if the younger date were correct, Kabwe 1 would be from a population exhibiting archaic cranial morphology that is cotemporaneous with at least the population represented by the Moroccan site of Jebel Irhoud (Hublin et al., 2017). Thus, Kabwe 1 may represent a broadly ancestral group relative to H. sapiens or a potential sister group. In either scenario, some shared derived traits may be expected in a physiologically important region such as the osseous nasopharyngeal boundaries and CET. Petralona 1 has also been identified previously as bearing close morphological similarity to Kabwe 1 (e.g., Freidline et al., 2012) and was thus included here.

Hypothesis 2 would be accepted if Kabwe 1 and Petralona 1 fell within the *H. sapiens* range of variation in measures of shorter relative CET length, more vertical CET orientation, and vertical medial pterygoid plate orientation relative to *H. neanderthalensis*, who exhibit differences from *H. sapiens* in these measures. This hypothesis would also be accepted if a 3D geometric morphometric analysis of the osseous nasopharyngeal boundaries showed Kabwe 1 and Petralona 1 plotting among *H. sapiens* to the exclusion of other fossil groups such as *H. neanderthalensis*.

Hypothesis 3. *H.* sapiens and *H.* neanderthalensis are both autapomorphic relative to the putative ancestral condition represented by *H.* erectus sensu lato.

Little has been written on the postnasal airway of H. erectus. The basicranial axis has been described as less flexed than among H. sapiens (Maier & Nkini, 1984; Weidenreich, 1943) and the superior root of the pterygoid plates on the Javanese Solo (Nandong) Skulls VI and XI as absolutely broader and more hypertrophied (Weidenreich, 1951). A Eustachian process (also called supratubal or infratubal process) is present among D2700 from Dmanisi, KNM-ER 3733 and 3883, Nandong 7, Sangiran 17, and Zhoukoudian Skull III (Anton, 2003; Delson et al., 2001; Rightmire, 1990; Rightmire et al., 2006; Weidenreich, 1943, 1951). This latter structure is a primitive mammalian trait (Cave, 1979) found among australopith-grade hominins (Ahern, 1998) and nonhuman primates (e.g., Doyle & Rood, 1979, 1980). Its presence among H. erectus suggests an ancestral pattern of tensor veli palatini (TVP) attachment (see Dean, 1982, for a full description of the nonhuman hominoid condition). Given the presence of some primitive postnasal traits and the likely origin of mPH from some population of H. erectus sensu lato, this group was used to represent the ancestral condition.

Hypothesis 3 would be accepted if *H. sapiens* and *H. neanderthalensis* differed consistently from *H. erectus* in possessing relatively shorter, broader nasopharyngeal morphology or if *H. erectus* individuals fell outside the *H. sapiens* and *H. neanderthalensis* ranges of variation in these measures. All nonhuman hominoids exhibit taller, narrower nasopharyngeal morphology relative to *H. sapiens* (Pagano & Laitman, 2015) and this is the probable ancestral condition that is expected among *H. erectus*.

Beyond the aforementioned analyses of phylogenetic polarity, we further discuss the functional implications of the observed variation among fossil hominin species.

2 | MATERIALS

2.1 | Fossil specimens

The following fossil hominins were used in this study (Table 1): *H. neanderthalensis* (Forbes' Quarry 1, La Chapelle aux Saints 1, La Ferrassie 1, Monte Circeo 1, and Saccopastore 1), mPH (Atapuerca 5, Kabwe 1, Petralona 1, and Steinheim 1), and two *H. erectus* crania (KNM-ER 3733 and Sangiran 17). Originals were examined by the authors (Laitman et al., 1979; Pagano, 2014; Pagano et al., 2019) with the exception of Sangiran 17. These fossil specimens were selected due to their nasopharyngeal boundaries and basicrania being, at least partly, intact. Fossil specimens were studied at the Natural History Museum (London), the Museo Nazionale Preistorico Etnografico Luigi Pigorini (Rome), Aristotle

University (Thessaloniki, Greece), Staatliches Museum für Naturkunde (Stuttgart, Germany), Institut für Anthropologie und Humangenetik der Universitat Tubingen (Tubingen, Germany), and the Musée de l'Homme (Paris).

The protocol of the current study derives from that in the study by Pagano (2014) and Pagano et al. (2019). Only specimens with a maximum of one missing midline landmark and one bilaterally missing pair of landmark locations at either the superior-most or inferior-most point on the medial pterygoid plate posterior edge were included. The thin-plate spline procedure of the "estimate.missing" function (Gunz et al., 2009; Sherratt, 2015) in the R statistical package Geomorph (Version 3.3.2; Adams et al., 2021) was used to estimate the positions of missing landmarks. Where possible, data collection commensurate with the current study's protocol was performed on original specimens (i.e., Forbes' Quarry 1, Monte Circeo 1, Kabwe 1, Petralona 1, and Steinheim 1) with others that could not be accessed to employ this protocol assessed instead on casts (Saccopastore 1 and Sangiran 17) or by virtual models derived from micro-CT scanning (La Chapelle aux Saints 1, La Ferrassie 1; both have been on display and not available for direct study), virtual models derived from CT scanning (KNM-ER-3733), and stereolithography (Atapuerca 5).

2.2 | Fossils not previously described in protocol

The degree of preservation of the medial pterygoid plates and other bony nasopharyngeal boundaries and the method by which the locations of missing or damaged landmarks were estimated have been described in some of the specimens and will not be repeated here (Pagano, 2014; Pagano et al., 2019, 2021). Those not previously described are discussed in detail below.

2.2.1 | La Chapelle aux Saints 1

A virtual specimen derived from high-quality micro-CT scanning of this specimen was produced at the Musée National d'Histoire Naturelle (Paris) (isometric data with a resolution of 0.123 mm for the complete skull). This micro-CT slice stack was rendered into a more manageable .PLY file format as this study's protocol required only surface morphology. Collection of landmark coordinate data was done in the Stratovan Checkpoint program (Stratovan Corporation, 2021). Enough of the boundaries of the bony Eustachian tube orifices on the left and right sides are preserved to estimate with confidence their



TABLE 1 The sample of fossil specimens used in the study

Specimens	Geological age	Method of data collection
Forbes' Quarry 1	Unknown	Original fossil; Natural History Museum, London
La Chapelle aux Saints	56-47 ka (Rendu et al., 2014)	micro-CT
La Ferrassie 1	52-45 ka (Talamo et al., 2020)	micro-CT
Monte Circeo 1	60–74 ka (Grün & Stringer, 1991), 44 ± 5 to 62.6 ± 6 (Schwarcz et al., 1991)	Original fossil; Museo Nazionale Preistorico Etnografico di Luigi Pigiorini
Saccopastore 1	120–130 ka (Grün, 1996)	Cast
Atapuerca 5	500–600 ka (Bischoff et al., 2007), 455 \pm 17 ka (Demuro et al., 2019)	Stereolithograph
Kabwe 1	202–235 ka (Barham & Smart, 1996), 500–700 ka (Avery, 2002), 300 ka (Grün et al., 2020)	Original fossil; Natural History Museum, London
Petralona 1	209-371 ka (Shen & Yokoyama, 1984), 150–250 ka (Grün, 1996)	Original fossil; Aristotle University of Thessaloniki, Greece
Steinheim 1	225 ka (Grün, 1996)	Original fossil; Staatliches Museum für Naturkunde (Stuttgart, Germany), formerly at Institut für Anthropologie und Humangenetik der Universitat Tubingen (Tubingen, Germany)
KNM-ER 3733	1.63 ma (Lepre & Kent, 2015)	CT
Sangiran 17	1.51-0.9 ma (Zaim et al., 2011)	Cast

locations. The location of hormion is identifiable from the fossa on the basisphenoid where the vomeral alae articulate. The posterior-most midline rim of this fossa was used to estimate the position of hormion. Most of the span of the palatine horizontal plates are missing despite the continued presence of the left and right palatine processes with the greater and lesser palatine foramina. However, segments of the palatine bones that articulate with isolateral alveolar processes are still present. These were used to assess the horizontal plane occupied by the hard palate while the coronal plane intersecting the left and right pyramidal processes indicated the posteriormost limit of the hard palate. The left medial pterygoid plate is near completely missing, whereas the right medial pterygoid plate is still present. Left-side landmarks coordinates were estimated using the "estimate. missing" function in R.

2.2.2 | La Ferrassie 1

As with the La Chapelle aux Saints 1 specimen, data from La Ferrassie 1 were derived from a high-quality virtual model derived from micro-CT scanning at the Musée National d'Histoire Naturelle (Paris) (isometric data with a resolution of 0.132 mm). Landmark

coordinate data were collected from a .PLY rendering of the micro-CT slice stack via the Stratovan Landmark program. As with La Chapelle aux Saints 1, the homologue of the H. sapiens sphenoid spine was visible and contacted the petrous temporal bones on both the left and right sides. The inferior lip of the osseous Eustachian tube orifice lies just superior and anterior to this junction and the landmark representing this structure was digitized here. Regarding the medial pterygoid plates, the left side was nearly intact while the right side was heavily damaged. Thus, missing landmarks on the superior-most edge and inferior limit of the scaphoid fossa were estimated using the "estimate.missing" function in R as was the position of hormion. The entire basisphenoid and ethmoid bones were also missing, as was the majority of the nasal cavity boundaries. The horizontal plates of the palatine bones were mostly missing but a small portion of their articulations with the alveolar processes were present bilaterally. This allowed for the estimation of the transverse plane of staphylion while, as with La Chapelle aux Saints 1, the coronal plane intersecting the left and right pyramidal processes was used to estimate the anteroposterior placement of staphylion, which was estimated ultimately at the intersection of these two planes.

2.2.3 | KNM-ER 3733

A virtual model derived from CT scanning (with a resolution of 0.3 mm and slice thickness of 0.5 mm) was accessed from the virtual collection of the Musee de l'Homme. The osseous Eustachian tube orifice boundaries were well preserved as was the superior-most portion of the left-side medial pterygoid plate posterior edge. However, the midpoints on the left and right medial pterygoid plate posterior edges (corresponding to the level of the scaphoid fossa inferior border) and the right-side inferior end of the medial pterygoid plate were missing and had to be reconstructed. Thus, neither medial pterygoid plate was preserved along its full superoinferior extent. The left- and right-side inferior-most points on the medial pterygoid plate posterior edge were missing and need to be reconstructed. The horizontal plates of the palatine bones were also missing but staphylion was estimated at the intersection of the transverse plane through the maxillary palatine processes and the perpendicular coronal plane passing through the anterior boundary of the left-side palatine pyramidal process.

2.2.4 | Sangiran 17

A virtual cast from Duke University, was downloaded from Morphosource.com. A 3D laser scanner was used to create a .PLY file representing the external cranial surface and landmark placement was performed in the Stratovan Checkpoint software.

The external osseous Eustachian tube orifices were present but an extremely large infratubal process made the position of the inferior lip of the orifice difficult to find. Instead, the point at which the infratubal process meets the rim of the osseous orifice anterolaterally was used. This landmark lies close enough to the one used on hominin crania lacking a well-expressed infratubal process that it can function as a homologous landmark. The superior-most points of contact of the medial pterygoid plates with the basicranium exhibit heavy damage but their positions were still estimable bilaterally. The inferior-most point on the right-side medial pterygoid plate posterior edge was estimable at the same transverse plane as the remaining portions of hard palate but the contralateral landmark was not present. Most of the medial pterygoid plates were almost completely missing bilaterally, including the scaphoid fossa and landmark representing the point at which the common tendon of the TVP muscle forms.

Staphylion was estimated in the midsagittal plane, intersecting the coronal plane passing through the posterior-most points at which the remaining portion of right palatine horizontal plate articulates with the alveolar process of the maxilla. The basicranial midline was in better condition with hormion visible as the superiormost portions of the vomeral alae remain preserved as they meet the basisphenoid bone.

2.3 | Contemporary human populations

The morphology of Neanderthals, mPH, and H. erectus were assessed alongside a developmental series of contemporary human populations (used here to represent H. sapiens) ranging in age from newborns to adults (all assessed directly by AP on original specimens). Adults in the growth series were used for direct morphological comparison to assess both functional and phylogenetic differences with the fossil specimens. The nonadults in the sample are also informative to functional analyses as newborns model anatomically the configuration of a vertically short, broad airway in combination with basicranial nonflexion and horizontal orientation of the choanae and CET (see Pagano et al., 2021). Any morphological similarities to newborn H. sapiens have functional implications on the upper respiratory tract (e.g., Laitman et al., 1979; Pagano et al., 2019) that may contribute to understanding of differences in character state among groups. This subsample was thus used in the Analysis of each linear measurement (see below).

The adult specimens (n = 180) were from the American Museum of Natural History Division of Anthropology and represent a geographically diverse group of crania including Alaskan Inuit, Aleutian Islander, Australian, Chinese, Indian (Mysore), Northern European, and West African (Table 2). There is a skew toward Alaskan and Aleut crania (n = 58 and n = 14, respectively), thus a larger proportionof this sample represents Arctic populations. The individuals were from preindustrial societies with no access to modern modes of transportation, likely minimizing the impact of geneflow and maximizing morphological diversity within the pooled sample. It must be noted that most of the sample is either male (n = 76) or of unknown sex (n = 71)with fewer representing females (n = 33). To address the potential confounding effects of sexual dimorphism, a series of Student's t-tests were performed comparing the male and female values for each univariate measure (see Section 3). There were no significant (p < 0.05) sex differences in these measures, indicating that sexual dimorphism, or the presence of specimens of unknown sex, did not influence variation within the *H. sapiens* sample.

The nonadult specimens are from the Spencer R. Atkinson Collection of the University of the Pacific School of Dentistry (San Francisco, California). While the nonadult specimens (Table 3) are also a geographically

Population	Males	Females	Unknown	Sample size
Alaska	9	11	38	n = 58
Aleutian Islands	7	4	3	n = 14
Australia	16	2	1	n = 19
China (South East)	13	1	1	n = 15
India (Mysore)	7	8	4	n = 19
Northern Europe (Germany)	12	2	4	n = 18
West Africa	12	5	0	n = 17
Unknown provenience	0	0	20	n = 20
Total adult sample	76	33	71	n = 180

TABLE 2 Composition of adult human sample

TABLE 3 Composition of growth series

Growth stage	Sample size	Definition of stage
Stage 1	n = 28	Edentulous newborns
Stage 2	<i>n</i> = 126	Only deciduous dentition erupted
Stage 3	<i>n</i> = 63	Between eruption of the first and the second permanent maxillary molars
Stage 4	<i>n</i> = 20	Between eruption of the second and the third permanent maxillary molars
Stage 5	n = 180	After eruption of the third permanent maxillary molars OR obliteration of spheno- occipital synchondrosis
Total modern humans	n = 417	Sum of all growth stages

diverse group (n=237) from the United States, Europe, China, and South America, they were not identified by individual provenience or sex (Dechant, 2000; Pagano et al., 2017, 2019, 2021). Thus, this sample cannot be used to assess population differences or sex differences in cranial growth.

All individuals were assigned a developmental stage based on dental eruption. Stage 1 individuals were edentulous newborns, Stage 2 spanned the period of time during which the deciduous dentition erupted until the eruption of the first maxillary molar, Stage 3 beginning at the eruption of the second maxillary molar and ending at the eruption of the second permanent maxillary molar and ending at the eruption of the second permanent maxillary molar, and Stage 5 beginning at either the eruption of the third maxillary molar, or the obliteration of the sphenooccipital synchondrosis. These growth stages have been used previously in studies of basicranial and facial

development and are known to correspond to periods of largescale cranial growth changes (Ashton, 1957; Bolter & Zihlman, 2003; Hellman, 1927; Laitman et al., 1979; Pagano et al., 2017, 2019).

3 | METHODS

Methods are adapted from Pagano et al. (2019, 2021). A total of 35 landmark coordinates (Figures 3-5, Table 4; see Pagano & Laitman, 2015, for a statement on interand intraobserver error) were collected from the facial skeleton and basicranium, including the nasopharyngeal boundaries, basicranium, CET floor, and dilator tubae muscles (Figure 6) using the "Eustachian Point" of Pagano (2014) and Pagano et al. (2017, 2019) to define the location of the osseous Eustachian tube orifice at its inferior lip (Figure 5). This lip usually lies in close proximity to the point of contact of the sphenoid spine (or its homolog) with the petrous temporal bone. It is also worth noting that facial landmarks are included as the proportions of the facial skeleton are functionally related to the morphology of the upper respiratory tract (Pagano & Laitman, 2015), of which the boundaries of the piriform aperture and oral cavity are components. They were selected so that linear measures of the osseous nasopharynx could be scaled more accurately over the size of the entire upper respiratory tract, including the facial skeleton and basicranium (see Section 3.1).

All morphological traits are here represented by coordinate data. As per our protocol, a specimen was considered sufficiently complete for inclusion in this study if all but one bilateral nasopharyngeal landmark location was present and if no more than one midline nasopharyngeal landmark location was absent. Two separate analyses were performed, a traditional morphometric analysis of univariate measures and a three-dimensional geometric morphometric analysis.

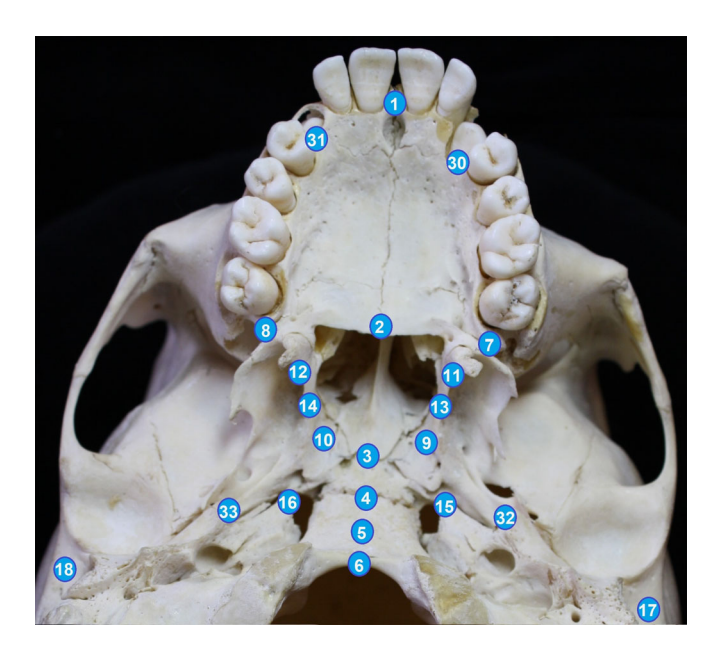


FIGURE 3 Basal landmarks used in Analysis 1. Only a subset of these (n = 11) were used in the principal components analysis of Analysis 2

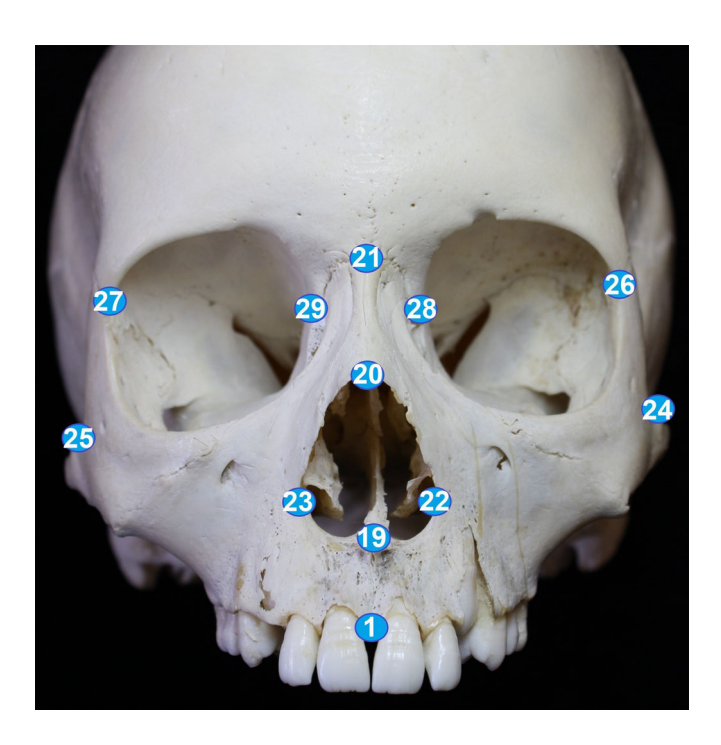


FIGURE 4 Frontal landmarks used in analysis 1

3.1 | Analysis 1—Univariate measures

Univariate measures are scale-free with all lengths representing relative dimensions as they are derived from coordinate data scaled over centroid size (the square root of the sum of squared distances from each landmark to the mean coordinate value). The following measures are

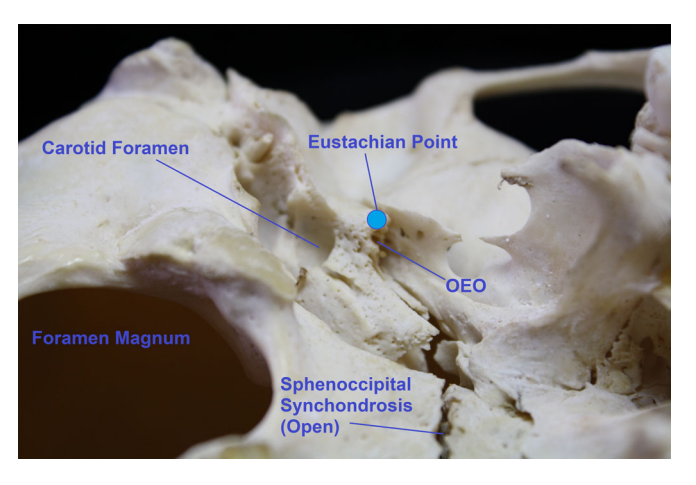


FIGURE 5 The location of the junction between the osseous and cartilaginous portions of the Eustachian tube, or Eustachian point, is represented by a landmark at the inferior-most point on the lip of the osseous orifice (OEO)

all illustrated in the work of Pagano et al. (2017, 2019). They are relative length and orientation of (A) the CET, (B) the dilator tubae, (C) the choanae, (D) the basicranial midline, and (E) facial kyphosis. The location of the osseous Eustachian tube orifice was represented by a landmark at its inferior lip, the Eustachian point (Landmarks 32 and 33). All bilateral measures were calculated as the average of left- and right-side values. Some measures of orientation were calculated using the Frankfort Horizontal Plane, which was defined using the three coordinates of right porion (Landmark 17), left porion (Landmark 18), and right zygorbitale (Landmark 34). As some adult *H. sapiens* crania did not have the position of right zygorbitale digitized, a smaller subset of the sample was used for aspects of Analysis 1 reliant on these measures.

- A. *CET relative length* was the measure between the Eustachian point (Landmarks 32 and 33) and the inferior-most point on the medial pterygoid plate posterior edge (Landmarks 11 and 12). This distance represents the *CET floor vector*. *CET orientation* was calculated using four separate measures:
 - Measure 1 of CET orientation calculated as the angle between the chord intersecting left and right Eustachian points and the isolateral CET floor vector. This measure represents the degree to which the CET is oriented coronally or sagittally along a mediolateral axis.
 - Measure 2 of CET orientation calculated as the angle of intersection of the line passing through the superior-most (Landmarks 9 and 10) and inferior-most points (Landmarks 11 and 12) on the medial pterygoid plate posterior edge with the Frankfurt Horizontal Plane. This measure



TABLE 4 Landmarks were selected from the facial skeleton and upper respiratory tract

- 1. Prosthion
- 2. Staphylion
- 3. Hormion
- 4. Sphenobasion
- 5. The point indicating the midline position of the pharyngeal tubercle, estimated as one third of the distance from endobasion to hormion when the tubercle was not visible
- 6. Endobasion
- 7. Left most posteroinferior point on the alveolar process of the maxilla
- 8. Right most posteroinferior point on the alveolar process of the maxilla
- 9. Left superior-most point on the posterior margin of the medial pterygoid plate
- 10. Right superior-most point on the posterior margin of the medial pterygoid plate
- 11. Left inferior-most point on the posterior margin of the pterygoid plate
- 12. Right inferior-most point on the posterior margin of the medial pterygoid plate
- 13. Left lateral-most midpoint on the choanal margin (approximating the level of the scaphoid fossa inferior boundary)
- 14. Right lateral-most midpoint on the choanal margin (approximating the level of the scaphoid fossa inferior boundary)
- 15. Left anteromedial-most point on basal surface of petrous temporal bone
- 16. Right anteromedial-most point on basal surface of petrous temporal bone
- 17. Left porion
- 18. Right porion
- 19. Nasospinale
- 20. Rhinion
- 21. Nasion
- 22. Left nasolaterale
- 23. Right nasolaterale
- 24. Left jugale (the point in the greatest depth of the notch between the temporal and frontal processes of the zygomatic bone)
- 25. Right jugale (the point in the greatest depth of the notch between the temporal and frontal processes of the zygomatic bone)
- 26. Left frontomalare orbitale
- 27. Right frontomalare orbitale
- 28. Left maxillofrontale
- 29. Right maxillofrontale
- 30. Left point on the internal alveolar margin posterior to the maxillary canine
- 31. Right point on the internal alveolar margin posterior to the maxillary canine
- 32. Left inferior-most point on the inferior lip of the osseous Eustachian tube orifice
- 33. Right inferior-most point on the inferior lip of the osseous Eustachian tube orifice

Note: Bolded landmarks were utilized in both Analysis 1 of right-side and midline landmark coordinates and in Analysis 2 of bilateral landmark coordinates. Zygorbitale was included only in calculating two angular measures within Analysis 2 but not during scaling over centroid size for either Analysis 1 or Analysis 2 and was thus not included in this table.

- represents the orientation of the lateral CET lamina with which the medial pterygoid plate makes contact.
- Measure 3 of CET orientation calculated as the angle of intersection of the line passing through the inferior-most point on the medial pterygoid plate posterior edge (Landmarks 11 and 12) and the Eustachian point (Landmarks 32 and 33) with
- the Frankfort Horizontal Plane. This measure represents the orientation of the CET floor independent of the orientation of the medial pterygoid plates.
- Measure 4 of CET orientation calculated as the angle between the CET floor vector and the medial pterygoid plate posterior edge between its superiorand inferior-most points.

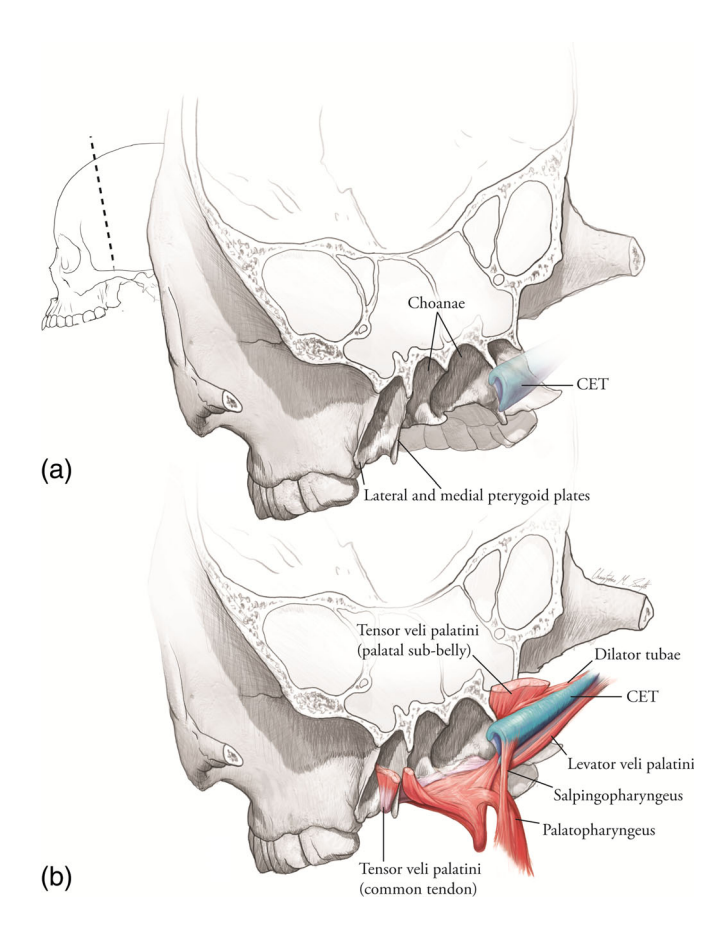


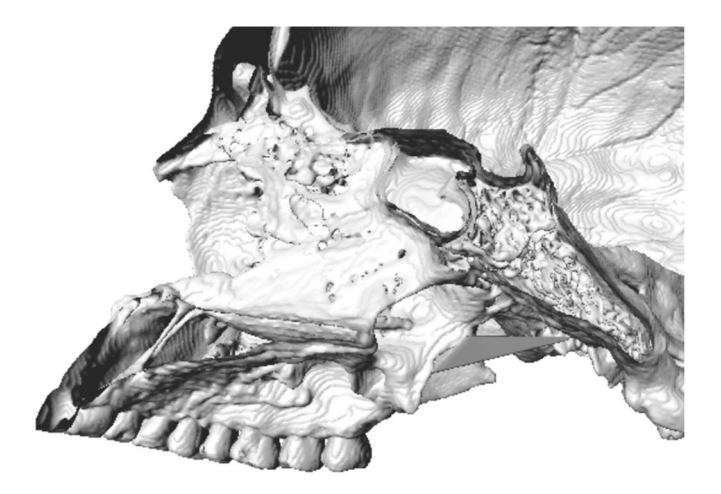
FIGURE 6 The tensor and levator veli palatini muscles are associated intimately with the cartilaginous Eustachian (pharyngotympanic) tubes (CETs). (a) Coronally sectioned cranium shown in posterolateral view; (b) same view with CET and nasopharyngeal musculature added. Note that the tensor veli palatini muscle has two contractile portions, the palatal sub-belly, and the dilator tubae

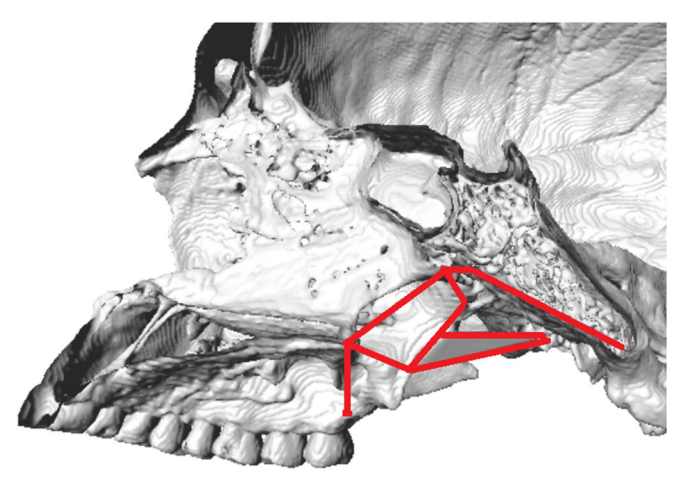
- B. Dilator tubae length was measured as the relative length between the Eustachian point and the point on the medial pterygoid plate posterior edge corresponding to the inferior limit of the scaphoid fossa (Landmarks 13 and 14). It was this latter landmark that represented the location at which the dilator tubae arm of the TVP muscle combined with the palatal sub-belly to form the common tendon. Orientation of the dilator tubae was calculated relative to the common tendon of the TVP muscle, spanning from the inferior boundary of the scaphoid fossa (Landmarks 13 and 14) to the inferior-most point on the medial pterygoid plate posterior edge (at the superior boundary of the pterygoid hamulus; Landmarks 11 and 12). Finally, a ratio of CET relative length/Dilator tubae relative length was calculated.
- C. Choanal height was measured both at the posterior vomeral surface (staphylion-hormion relative distance) and along the medial pterygoid plate posterior

- edge (from superior- to inferior-most points). Choanal width was measured both between the left- and right-side scaphoid fossa inferior boundaries (Landmarks 13 and 14) and superior-most points (Landmarks 9 and 10) along the medial pterygoid plate posterior edges. The former measure was also expressed as a choanal index relative to vomeral height [(width/height) \times 100].
- D. Choanal orientation was measured relative to the basicranial midline (hormion-sphenobasion chord) using both the posterior vomeral surface (staphylion-hormion-sphenobasion angle) and using midpoints of the left- and right-side inferior-most and superior-most points on the medial pterygoid plate posterior edges (Landmarks 9–10 midpoint and Landmarks 11–12 midpoint).
- E. Basicranial length was measured as the relative distance between hormion and endobasion.
- F. Facial kyphosis was measured here as the staphylion-hormion-sphenobasion angle. This measure is a departure from the original concept of facial kyphosis relative to endocranial cavity (Hofer, 1952; Ross & Ravosa, 1993; Starck, 1953), instead focusing on the relationship of the facial skeleton to the basicranium in the midsagittal plane.

3.2 | Analysis 2—Three-dimensional geometric morphometric analysis

A Generalized Procrustes Analysis and subsequent Principal Components Analysis (see review in Cooke & Terhune, 2015) was performed using only 11 right-side nasopharyngeal landmarks in the Morphologika2 (Version 2.5) software (Figures 4-6). Shape variation in Analysis 2 was visualized at first by wireframe models generated in Morphologika2 (Figure 7) outlining the choanae, CET, dilator tubae, and basicranial axis. Additional visualization was performed using the "warpmesh" function in the R packages Geomorph and Morpho. This process (described in detail by Pagano et al., 2019) entails acquiring a CT scan of the specimen closest to the mean shape, which was an Inuit cranium from Point Hope Alaska (991/481) from the American Museum of Natural History. This specimen was rendered into a .PLY file format to create a surface model and a red triangle was created in the program Geomagic between the medial pterygoid plate posterior edge and the Eustachian point to simulate the span of the CET and dilator tubae. This surface model was then warped to fit the landmark configuration of the consensus (or mean) shape, creating a mean warp. It was the mean warp that was, in turn, warped at each of the 11 landmark locations to fit the





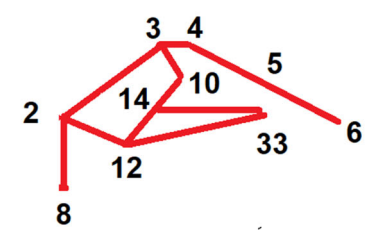


FIGURE 7 Variation along shape space in Analysis 2 was visualized, in part, via wireframe renderings. These wireframes represented the right-side maxillary tubercle, choana, cartilaginous Eustachian (pharyngotympanic) tube (CET), and basicranial midline

shapes representing the average adult *H. sapiens*, average Neanderthal, each of the mPH specimens, and KNM-ER 3733.

We chose not to include the nonadult *H. sapiens* in Analysis 2 as any morphological differences represented on the Principal Components Analysis (PCA) chart would not represent evolutionary relationships. The distinct shape configuration of the newborn osseous nasopharyngeal boundaries (Pagano et al., 2017, 2019) would obfuscate phylogenetically rooted shape differences among adult *H. sapiens* and fossil crania which, while

finer in absolute magnitude, are of greater evolutionary importance.

4 | RESULTS

4.1 | Analysis 1—Univariate measures

4.1.1 | *H. sapiens* autapomorphies

H. sapiens autapomorphies were identified relative to Neanderthals, mPH, and H. erectus in relatively low vomeral height, broad choanae (Figure 8a), vertical angulation of the medial pterygoid plate posterior edges relative to the basicranium (Figure 8b), and more coronally oriented CETs (Measure 1 of CET orientation, Figure 8c). These appear related to the general morphological pattern of basicranial flexion and an anteroposteriorly long, mediolaterally broad upper airway. The relative distance between hormion and endobasion (Figure 8d) is indeed longer among H. sapiens of all growth stages as all fossil specimens exhibit values lower than the H. sapiens average. Furthermore, most of the fossils lie within the extreme range of H. sapiens variation in this measure. These traits distinguish H. sapiens from H. neanderthalensis, mPH, and H. erectus as they all possess relatively (to H. sapiens) taller vomeral height, narrower choanae, more horizontal orientation of the pterygoid plate posterior edges relative to the basicranium and more sagittally oriented CETs.

4.1.2 | *H. neanderthalensis* autapomorphies

H. neanderthalensis autapomorphies relative to H. sapiens, mPH, and H. erectus include an obtuse angle of facial kyphosis (relative to the basicranial midline, Figure 9a) and midline choanal/vomeral orientation (Figure 9b) with all H. neanderthalensis lying above the adult H. sapiens mean. When calculated as a ratio, posterior vomeral edge height relative to medial pterygoid plate height (Figure 9c) was much higher among all H. neanderthalensis except La Ferrassie 1, for whom the position of hormion was reconstructed and a high value for choanal orientation relative to the other H. neanderthalensis specimens suggests that the position of staphylion in this specimen was calculated further anterior than it may have been in life. The two Western European mPH also exhibited high, Neanderthallike values, exceeding most H. sapiens, Kabwe 1, and Petralona 1. A high value suggests that the vomer is curved more horizontally over a longer distance as its inferior-most point is measured at the same transverse plane as that of the medial pterygoid plates. Such horizontal vomeral orientation is similar to the condition of infants and young

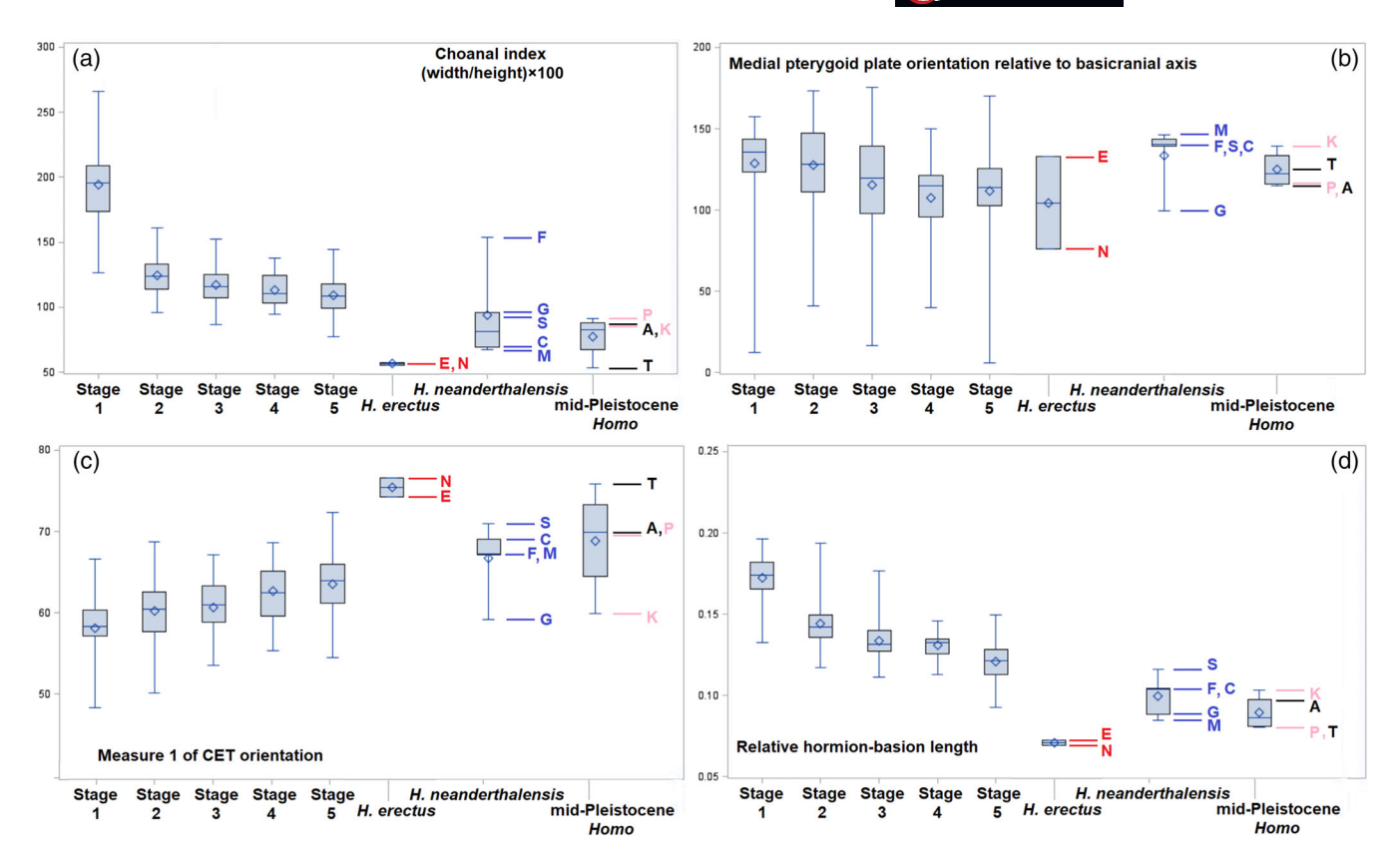


FIGURE 8 Box-whisker plots of univariate measures that distinguish *Homo sapiens*. Measures calculated from coordinate data scaled over centroid size. The mean is represented by the blue diamond and the edges of the box and whiskers represent 5%, 25%, 75%, and 95% quartiles. Fossils include Sangiran 17 (N), KNM-ER-3733 (E), La Chapelle aux Saints 1 (C), La Ferrassie 1 (F), Forbes' Quarry 1 (G), Monte Circeo 1 (M), Saccopastore 1 (S), Atapuerca 5 (A), Steinheim 1 (T), Kabwe 1 (K), and Petralona 1 (P). Stages 1–5 represent *H. sapiens* growth series from newborns (Stage 1) to adults (Stage 5)

children in the growth series. The medial pterygoid plates also appeared horizontally oriented (Measure 2 of CET orientation, Figure 9d) relative to *H. sapiens* but overlapped mPH and *H. erectus*. Relative length of the dilator tubae muscle (Figure 10a) was also greater among all *H. neanderthalensis* than the *H. sapiens* mean and all mPH crania, except for La Chapelle aux Saints 1. When expressed as a ratio, dilator tubae length relative to CET floor length (Figure 10b) is greater among all *H. neanderthalensis* specimens (except for La Chapelle aux Saints 1) than the adult *H. sapiens* mean but Kabwe 1 also plots in the *H. neanderthalensis* range for this measure.

4.1.3 | Characteristics of mPH sample

Regarding the relative length of the CET itself (Figure 11a), Kabwe 1, Petralona 1, and Atapuerca 5 exhibit low values such as those of adult *H. sapiens*, whereas Steinheim 1 exhibits a higher value, closer to those of *H. neanderthalensis*. However, other traits distinguish the pooled mPH sample from both *H. neanderthalensis* and

H. sapiens. These include extremely vertical medial pterygoid plate orientation relative to the Frankfort Horizontal Plane (Measure 3 of CET orientation, Figure 11b), lying at the extreme range of H. sapiens and H. neanderthalensis variation. The respective orientations of the dilator tubae (Figure 11c) and CET floor (Measure 4 of CET orientation, Figure 11d) relative to the medial pterygoid plates among most mPH specimens is horizontal as among H. sapiens newborns and infants in the growth series. This morphological configuration of horizontal dilator tubae and CET orientation relative to the medial pterygoid plate is absent among both H. sapiens and H. neanderthalensis and characterizes all mPH specimens except Atapuerca 5, which falls closer to the H. neanderthalensis mean in dilator tubae orientation.

4.1.4 | Distinguishing *H. erectus*

KNM-ER 3733 and Sangiran 17 exhibited extremely low values for relative choanal width, both at the reconstructed location of the scaphoid fossa inferior limit

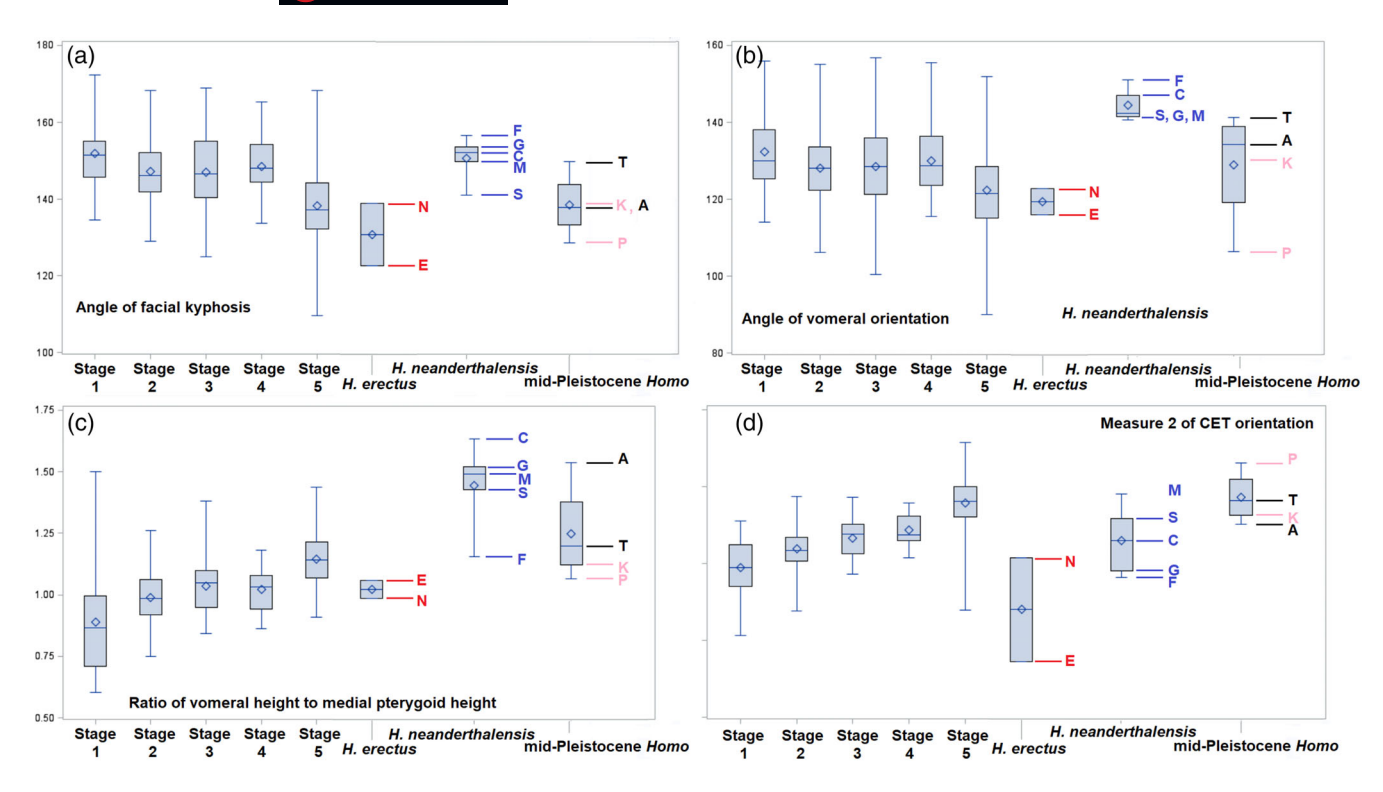


FIGURE 9 Box-whisker plots of univariate measures that distinguish *Homo neanderthalensis*. Measures are calculated from coordinate data scaled over centroid size. The mean is represented by the blue diamond and the edges of the box and whiskers represent 5%, 25%, 75%, and 95% quartiles. Fossils include Sangiran 17 (N), KNM-ER-3733 (E), La Chapelle aux Saints 1 (C), La Ferrassie 1 (F), Forbes' Quarry 1 (G), Monte Circeo 1 (M), Saccopastore 1 (S), Atapuerca 5 (A), Steinheim 1 (T), Kabwe 1 (K), and Petralona 1 (P). Stages 1–5 represent *Homo sapiens* growth series from newborns (Stage 1) to adults (Stage 5)

(Figure 12a) and at the superior choanal boundaries (Figure 12b). In these measures, both fell outside the mPH, H. neanderthalensis, and H. sapiens range. When expressed as a ratio of vomeral height, relative choanal breadth (Figure 8a) was still more narrow in these specimens than all other crania except Steinheim 1 (although the values of the latter specimen may be attributed, in part, to postmortem distortion). Relative distance between the left and right Eustachian tube osseous orifices (Figure 12c) was also the narrowest among the two H. erectus crania and hormionendobasion relative length (Figure 8d) was shorter than among any other specimen in the study. This morphology was accompanied by CETs with an extreme sagittal orientation (that is, their average angle of mediolateral rotation was extremely high, Figure 8c). Both specimens exhibited nearly identical values for CET orientation relative to the Frankfort Horizontal Plane (Figure 9d), lying less than 1.3 standard deviations below the adult H. sapiens mean (i.e., more horizontal). There were, however, other ways in which the two crania differed from each other. While KNM-ER-3733 had extremely vertical CET orientation relative to the medial pterygoid plates (Measure 4 of CET orientation, Figure 11d), Sangiran 17 exhibited a less extreme value, close to the H. sapiens adult mean. This may be

related to the extremely horizontal medial pterygoid plate orientation relative to the Frankfort Horizontal Plane (Measure 2 of CET orientation, Figure 9d) of KNM-ER-3733 whose value is the lowest of any specimen. Sangiran 17 also expressed a low value in this measure, at the extreme range of *H. sapiens* and *H. neanderthalensis* variation (over two standard deviations below the *H. sapiens* adult mean) but its value was not as extreme as that of KNM-ER-3733.

4.2 | Analysis 2—Generalized Procrustes analysis and principal components analysis of adult sample

Overall shape variation does not appear to be concentrated in any single shape vector as PC1 only comprises 21.2% of overall shape variance with PCs 2 and 3 comprising 17.2% and 9.29% of shape variance, respectively (Figures 7, 13, and 14). PC4 comprised 8.7% of shape variance and PC5 comprised 5.97% with no further PCs accounting for more than 5%. However, these did not reflect any meaningful aspect of shape variation and are thus not shown here.

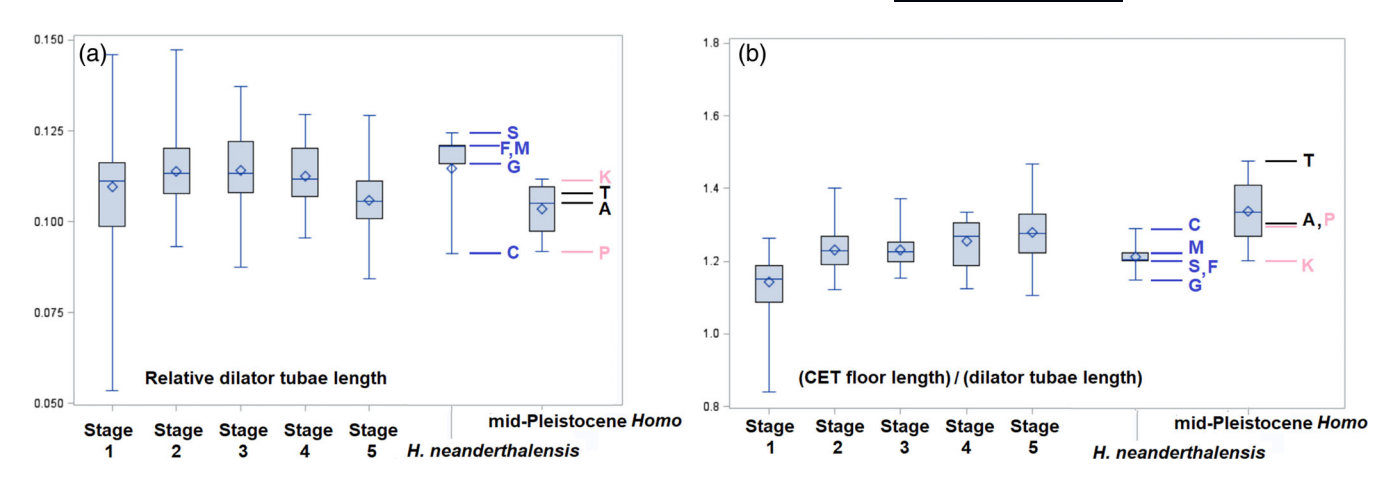


FIGURE 10 Box-whisker plots of univariate measures of relative dilator tubae length distinguishing *Homo neanderthalensis*. Measures are calculated from coordinate data scaled over centroid size. The mean is represented by the blue diamond and the edges of the box and whiskers represent 5%, 25%, 75%, and 95% quartiles. Fossil crania include La Chapelle aux Saints 1 (C), La Ferrassie 1 (F), Forbes' Quarry 1 (G), Guattarri 1 (M), Saccopastore 1 (S), Atapuerca 5 (A), Steinheim 1 (T), Kabwe 1 (K), and Petralona 1 (P). Stages 1–5 represent a *Homo sapiens* growth series ranging from newborns (Stage 1) to adults (Stage 5)

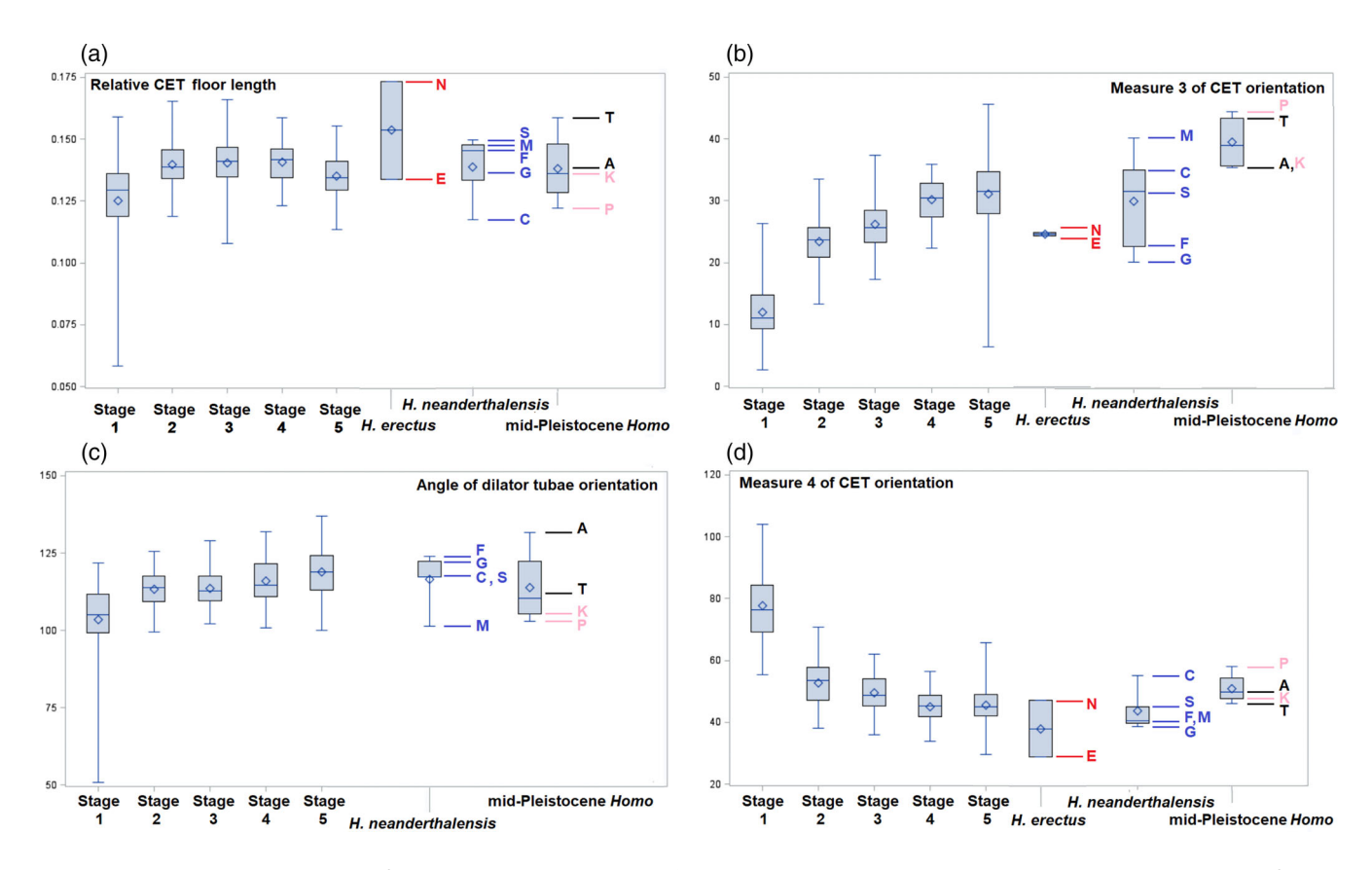
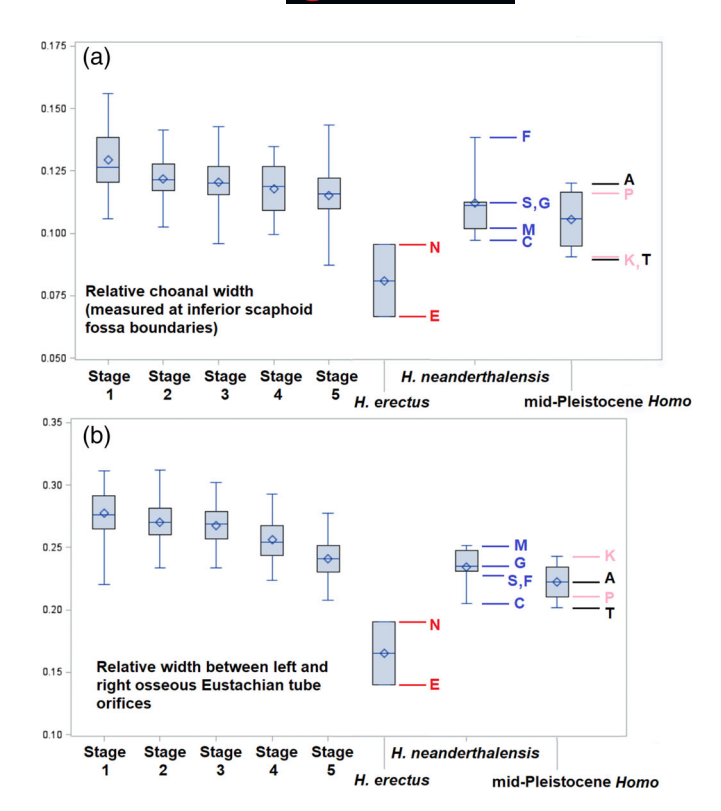


FIGURE 11 Box-whisker plots of univariate measures whose values distinguish mid-Pleistocene *Homo*. Measures are calculated from coordinate data scaled over centroid size. The mean is represented by the blue diamond and the edges of the box and whiskers represent 5%, 25%, 75%, and 95% quartiles. Fossils include Sangiran 17 (N), KNM-ER-3733 (E), La Chapelle aux saints 1 (C), La Ferrassie 1 (F), Forbes' Quarry 1 (G), Monte Circeo 1 (M), Saccopastore 1 (S), Atapuerca 5 (A), Steinheim 1 (T), Kabwe 1 (K), and Petralona 1 (P). Stages 1–5 represent *Homo sapiens* growth series from newborns (Stage 1) to adults (Stage 5)

Moving to the positive side of PC1 leads to basicranial retroflexion and horizontal orientation of the posterior vomeral surface and inferior portion of the medial pterygoid plate corresponding to the common TVP tendon. There is also lengthening of both the dilator tubae and CET floor and horizontal CET orientation. This



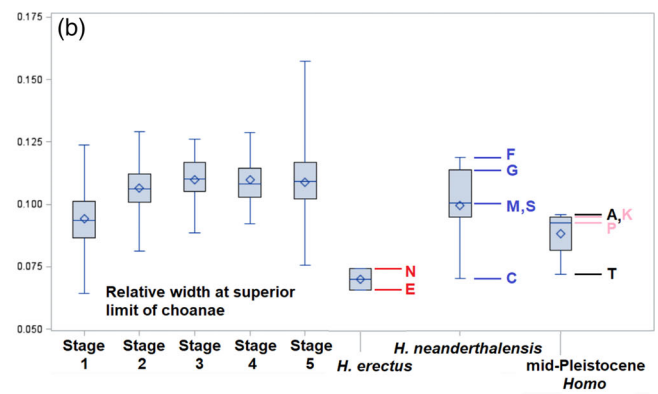


FIGURE 12 Box-whisker plots of univariate measures distinguishing *Homo erectus* sensu *lato*. Measures are calculated from coordinate data scaled over centroid size. The mean is represented by the blue diamond and the edges of the box and whiskers represent 5%, 25%, 75%, and 95% quartiles. Fossils include Sangiran 17 (N), KNM-ER-3733 (E), La Chapelle aux Saints 1 (C), La Ferrassie 1 (F), Forbes' Quarry 1 (G), Monte Circeo 1 (M), Saccopastore 1 (S), Atapuerca 5 (A), Steinheim 1 (T), Kabwe 1 (K), and Petralona 1 (P). Stages 1–5 represent *Homo sapiens* growth series from newborns (Stage 1) to adults (Stage 5)

morphological pattern was also visible in a warped mesh model (Figure 15; generated from warping a surface scan of the specimen closest to the mean shape into a target shape using landmark coordinate data) in which the average *H. neanderthalensis* exhibited extremely horizontal vomeral and CET orientation.

Moving toward the negative end of PC2 produces tall, narrow choanae, inferior displacement of the alveolar process of the maxilla relative to the hard palate, and horizontal CET floor orientation (Figure 13). Most H. neanderthalensis plot on the positive end of this axis while roughly equal proportions of the H. sapiens sample occur on either side of this axis. The fossil crania are separated well by PC2 with H. neanderthalensis occupying the positive end of the axis, mPH specimens dispersed still lower, and KNM-ER 3733 and Sangiran 17 occupying the negative extreme of this axis, lying completely outside the H. sapiens range. H. sapiens variation occurs in a tighter cluster along PC3 with La Ferrassie 1, Atapuerca 5, and Saccopastore 1 all lying at the negative side of the axis while La Chapelle aux Saints 1, Forbes' Quarry 1, Monte Circeo, and Petralona 1 plot at the positive side of the axis. Kabwe 1, KNM-ER 3733, Steinheim 1, Forbes' Quarry 1, and Sangiran 17 are within the range of *H. sapiens* variation on this vector. Movement toward the positive end of PC3 shows increasing length of the common TVP tendon, increased length of the CET floor, basicranial retroflexion, and vertical reorientation of the basicranium in midline.

Of note is that *H. sapiens* and *H. neanderthalensis* comprise distinct clusters on the chart of PC1 and PC2 values. All *H. neanderthalensis* specimens occupy the negative end of PC1 and tend to cluster closely except for Saccopastore 1, which appears to form a second cluster with Steinheim 1, Atapuerca 5, and KNM-ER 3733. Kabwe and Petralona lie within the *H. sapiens* cluster and Atapuerca 5 is at its extreme range, overlapping only one *H. sapiens* individual along PC1. The two *H. erectus* crania are the most distant from all other specimens, but Steinheim 1 approaches their position as it has the tallest, narrowest airway shape of any of the mPH specimens. Indeed, it appears to be the most robust specimen in this group.

4.3 | Identification of the Levator process: A previously undescribed structure in *H. neanderthalensis*

This process lies in the same anatomical position as the levator veli palatini muscle origin in *H. sapiens* (Figure 16). We

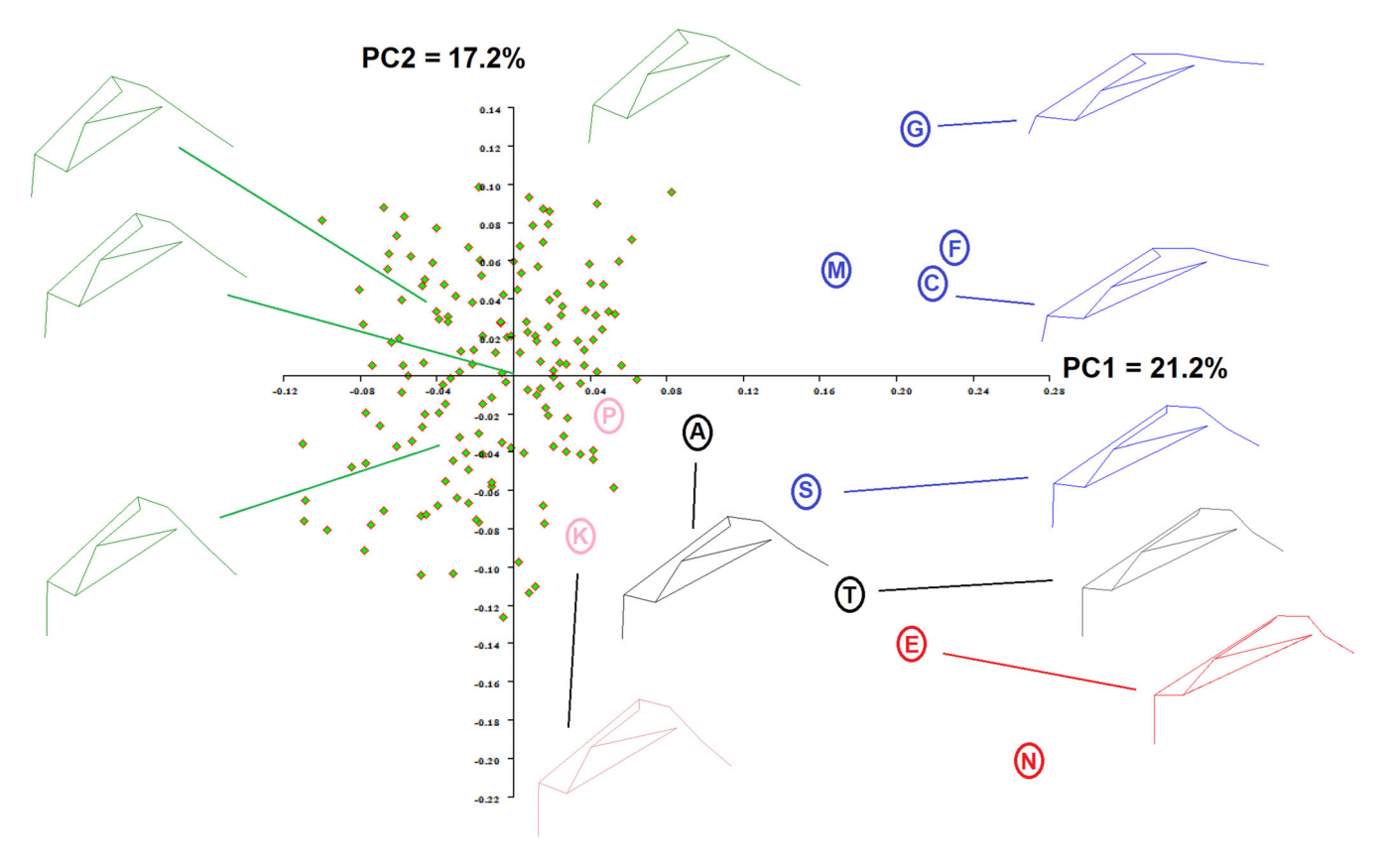


FIGURE 13 A principal components (PC) chart of the shape space generated from a generalized Procrustes analysis. Fossil crania include La Chapelle aux Saints 1 (C), La Ferrassie 1 (F), Gibraltar Forbes' Quarry 1 (G), Monte Circeo (M), Saccopastore 1 (S), Atapuerca 5 (A), Steinheim 1 (T), Kabwe 1 (K), Petralona 1 (P), KNM-ER 3733 (E), and Sangiran 17 (N). PCs 1 and 2 were close in the proportion of shape variance that they comprised. *Homo sapiens* and *Homo neanderthalensis* occupied different positions in shape space with Petralona 1 and Kabwe 1 falling into the *H. sapiens* cluster. Atapuerca 5 was intermediate in position between Petralona 1 and Saccopastore 1, whereas Steinheim 1 was intermediate in position between Saccopastore 1 and KNM-ER 3733

term this structure the "levator process." The apex points posteromedially with a rectangular fossa (levator fossa) on its medial surface that was the site of origin of the levator veli palatini muscle, close to the osseous Eustachian tube orifice. The levator process lies just posterior and medial to the large entoglenoid tubercle. This structure is best preserved in La Chapelle aux Saints 1 (Figure 17), where the outline of the fossa is observed. The morphology of this fossa suggests that La Chapelle aux Saints 1 possessed a broad, well-developed levator veli palatini muscle. The levator process of Guattari 1 (Figure 18) is present but smaller than that of La Chapelle aux Saints 1. Forbes' Quarry 1 also exhibits a levator process (Figure 19) but it appears eroded and damaged. Still, a portion of the levator fossa can be visualized just posterior to the osseous Eustachian tube orifice (which remains plugged with matrix).

5 | DISCUSSION

This discussion will begin by focusing on the two crown taxa, *H. sapiens* and *H. neanderthalensis*. We characterize

their respective morphologies (and autapomorphies relative to each other and other groups) and assess the condition of their last common ancestor by analyzing the pooled mPH group for traits in which both *H. sapiens* and *H. neanderthalensis* differ. Also included is a discussion of how mPH differs from *H. erectus* and the two-step process by which (1) mPH arose from *H. erectus* and (2) the *H. sapiens* and *H. neanderthalensis* evolutionary trajectories diverged from a common ancestral population of mPH.

5.1 | The condition of H. sapiens

H. sapiens can be characterized as exhibiting vertically short, mediolaterally broad choanae, vertically oriented medial pterygoid plates, coronally oriented CETs within the transverse plane, and relative elongation and flexion of the basicranial midline between hormion and endobasion. This morphological pattern is related to a well-expressed torus tubarius (or distal tip of the CET) as the choanae and nasopharyngeal boundaries extend far

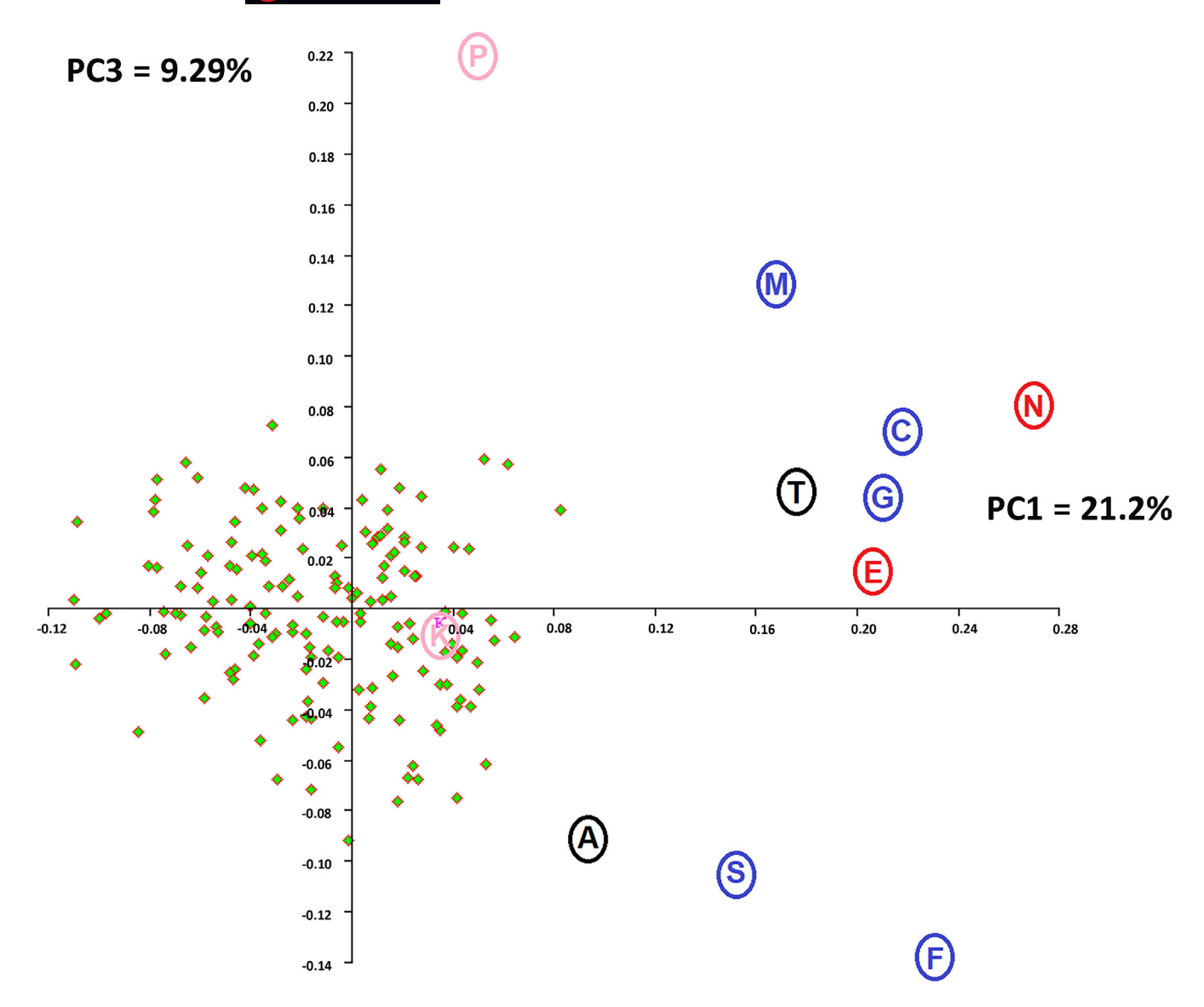


FIGURE 14 A principal components (PCs) chart of the shape space generated from a generalized Procrustes analysis. Fossil crania include La Chapelle aux Saints 1 (C), La Ferrassie 1 (F), Forbes' Quarry 1 (G), Monte Circeo 1 (M), Saccopastore 1 (S), Atapuerca 5 (A), Steinheim 1 (T), Kabwe 1 (K), Petralona 1 (P), KNM-ER 3733 (E), and Sangiran 17 (N). When PCs 1 and 3 are plotted together, Kabwe 1 is the sole fossil to lie within the *Homo sapiens* cluster. However, PC 3 alone does not serve to distinguish modern humans from the fossil crania

enough laterally that the pharyngeal end of the CET projects into the nasopharynx, creating a lateral pharyngeal recess (of Rosenmüller) posterior to it as an invagination forms between the posterior edge of the torus tubarius and the mucosa covering the superior pharyngeal constrictor muscle. All of the *H. neanderthalensis* and mPH overlap *H. sapiens* in measures of choanal width, with the exceptions of Kabwe 1 and Steinheim 1. While the latter specimen may be influenced by postmortem warping (see descriptions by Laitman et al., 1979; Pagano, 2014), the former exhibits extremely narrow choanae that could have led to a weaker torus tubarius expression in life.

H. sapiens also exhibit an autapomorphic feature in the sphenoid spine which is not present in any of the fossils except Kabwe 1 (Figure 20). However, Kabwe 1 still has its foramen spinosum at a (probably) primitive posteromedial position, resembling the condition of H. neanderthalensis (see Figure 18). H. sapiens, in contrast, has a foramen spinosum (as the name suggests) that traverses the sphenoid spine itself (see Figure 16). None of the other mPH specimens exhibits a sphenoid spine, making this feature a potentially shared derived trait among H. sapiens and the population represented by Kabwe 1, even if the latter does not exhibit the exact morphological configuration of H. sapiens.

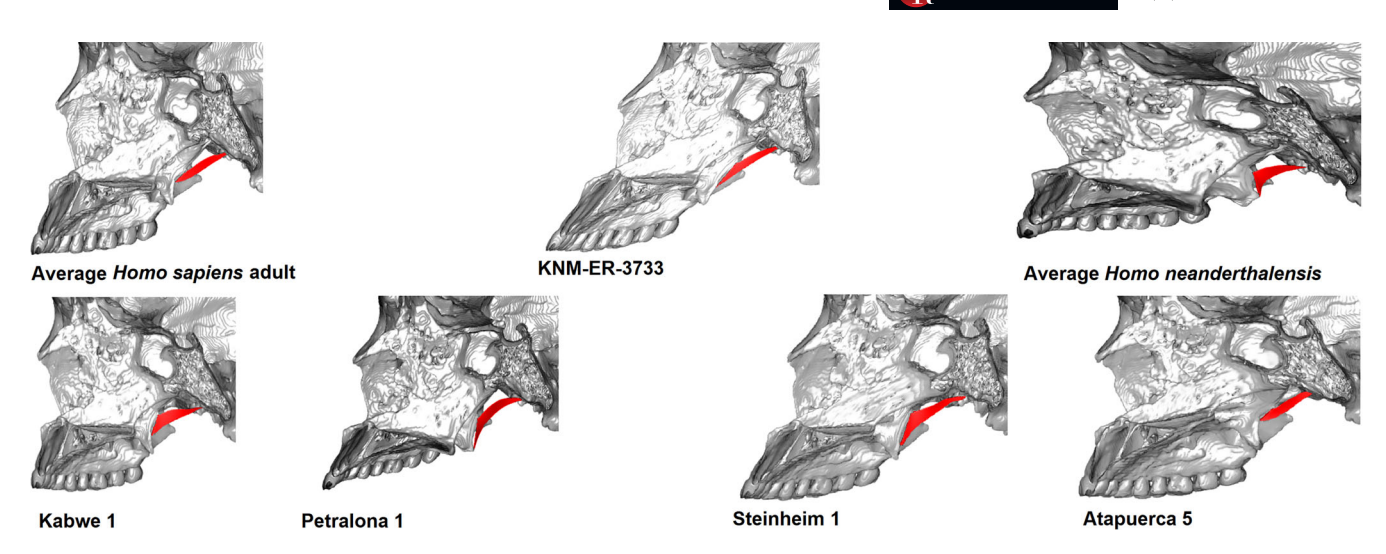


FIGURE 15 Shape variation along the shape space generated in Analysis 2 was visualized, in part, via the "warpmesh" function in the R package Geomorph. This process involved warping a consensus specimen (a surface model of a parasagittaly-sectioned cranium) to the respective shapes of the average *Homo sapiens*, average *Homo neanderthalensis*, each of the mPH crania, and KNM-ER 3733. The cartilaginous Eustachian (pharyngotympanic) tube (CET) is represented here by a red triangle spanning from the Eustachian point laterally to the inferior-most point and midpoint (approximating the scaphoid fossa inferior boundary) of the medial pterygoid plate. *Homo neanderthalensis*, Atapuerca 5, and Steinheim 1 can all be seen expressing more horizontal orientation of the vomer while only the *H. neanderthalensis* exhibit extremely horizontal CETs. KNM-ER 3733 exhibits the most vertically tall choanae and anteriorly rotated medial pterygoid plates

5.2 | The condition of the Neanderthal nasopharynx and its functional implications

Anterior displacement of the hard palate and inferior portion of the medial pterygoid plate represent among H. neanderthalensis a relatively longer soft palate with more hypertrophied palatal musculature. The additional presence of an enlarged process of levator veli palatini attachment further suggests a more hypertrophied muscle necessitated by a longer, more hypertrophied soft palate. The presence of a clearly recognizable levator origin lateral to the osseous Eustachian tube and, by extension, lateral to the dilator tubae muscle among H. neanderthalensis suggests that this configuration is a shared derived trait with H. sapiens that probably evolved among their common ancestor in the early Middle Pleistocene. A lateral origin of the levator veli palatini (relative to the TVP) was identified previously by Dean (1982) as a soft tissue trait distinguishing H. sapiens from the great apes. However, the presence of a levator process appears autapomorphic among H. neanderthalensis as this trait was not found among H. sapiens, mPH, or H. erectus crania. The levator process, along with the other exclusively H. neanderthalensis traits described in Analyses 1 and 2, appears to be yet another piece of evidence that H. neanderthalensis should be considered a distinct species.

In contrast to the *H. neanderthalensis* condition, *H. sapiens* exhibit a crest of variable thickness between the osseous Eustachian tube orifice and carotid foramen.

This crest extends anteromedially from the inferior boundary of a variably present impression of the levator veli palatini muscle origin on the temporal bone (Rohan & Turner, 1956). However, this condition may be absent among some individuals for whom the levator veli palatini muscle takes origin on the fibrous junction of the CET and its osseous temporal bone orifice (Huang et al., 1997). Such a crest could not form on the Neanderthal temporal bone as the enlarged entoglenoid tubercle limits it anteriorly.

An enlarged levator veli palatini muscle in *H. neanderthalensis* may have been necessitated by the relatively anterior position of the hard palate and overall nonflexed appearance of the postnasal airway between staphylion and sphenobasion, producing an anteroposteriorly longer space for the soft palate to fill between its anterior attachment to the palatine bones and its posterior limit at the level of the pharyngeal wall (represented by the coronal plane through the spheno-occipital synchondrosis; Takagi et al., 1962). A muscle that must act across a longer distance has less mechanical advantage and thus a thickened, well-developed levator veli palatini muscle may have arisen as a compensatory mechanism among Neanderthals.

Morphological differences between *H. neanderthalensis* and *H. sapiens* may have also resulted in functional differences in the soft palate and CET. The extreme length of the *H. neanderthalensis* dilator tubae relative to the CET floor may be of special importance as the former structure is the

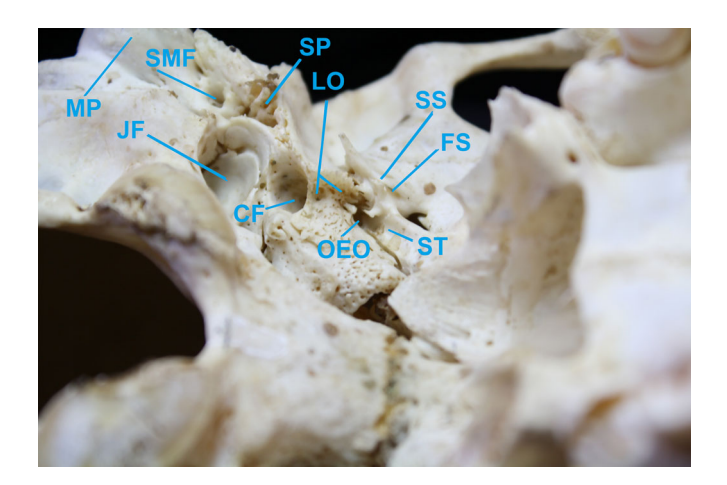


FIGURE 16 Basal view of the right-side temporal bone of a 12–17 year-old adolescent from the Spenser R. Atkinson Collection (D56). A ridge forms at the inferior limit of the origin of the levator veli palatini muscle (LO). The ridge spans between the osseous Eustachian tube orifice (OEO) and the carotid foramen (CF). A sulcus tubarius (ST) associated with the proximal-most portion of the cartilaginous Eustachian tube (or isthmus) extends from the OEO toward the medial pterygoid plate medially. Other structures visible are the sphenoid spine (SS), foramen spinosum (FS), mastoid process (MP), stylomastoid foramen (SMF), base of broken styloid process (SP), and jugular foramen (JF)

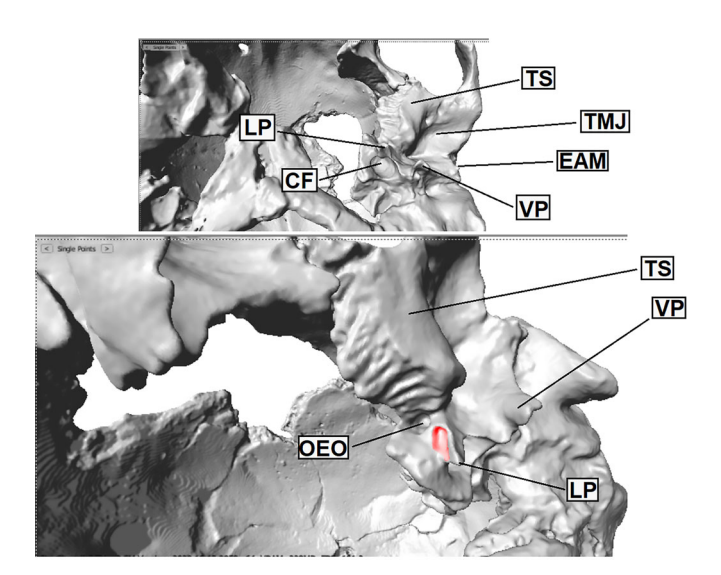


FIGURE 17 (Top) Basal view of the left-side basicranium of the La Chapelle aux Saints 1 Neanderthal cranium. This image was generated from a micro-CT scan (see Section 2 for details). Structures include squamous portion of the temporal bone (TS), temporomandibular joint surface (TMJ), external auditory meatus (EAM), vaginal process surrounding a broken styloid process (VP), carotid foramen (CF), origin of the levator veli palatini muscle (or levator process, LP). The specimen is laterally and inferiorly rotated (bottom) to expose the anterior surface of the LP, levator fossa (in red), and the osseous Eustachian tube orifice (OEO). This specimen exhibits the best-preserved LP

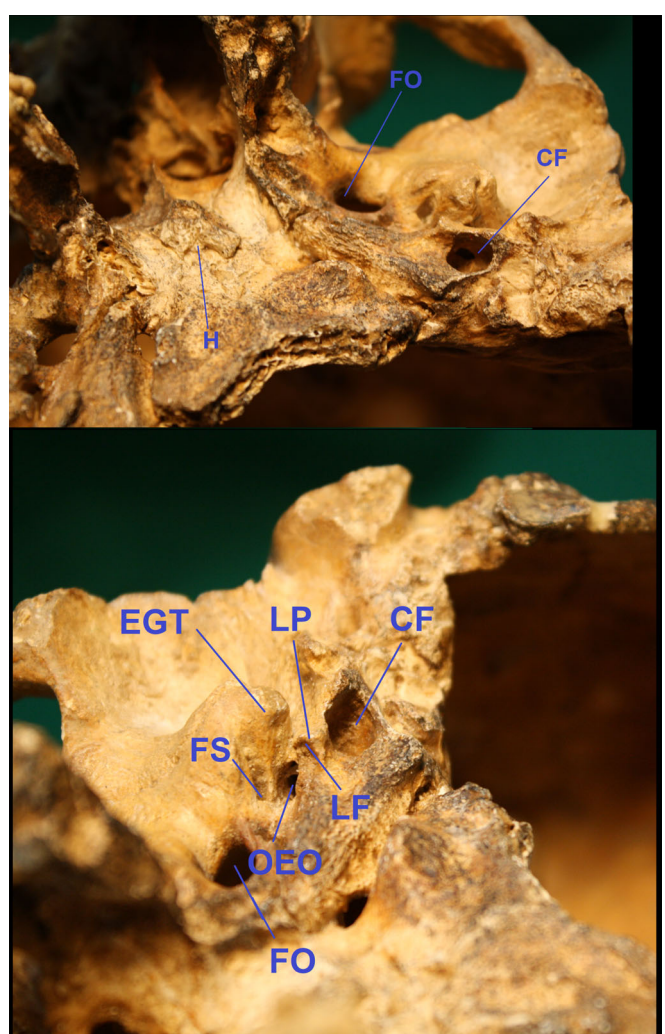


FIGURE 18 (Top) Basal view of the left-side basicranium of the Monte Circeo 1 Neanderthal cranium. Visible from this orientation are hormion (H, between the two vomeral alae), foramen ovale (FO), and carotid foramen (CF). When rotated 90° to the right (bottom), the spatial relationships of the levator process (LP) and levator fossa (LF) with the entoglenoid tubercle (EGT), foramen spinosum (FS), and osseous Eustachian tube orifice (OEO) become visible. The LP on this specimen exhibits some postmortem damage but is still observable

sole dilator of the latter structure and this relationship has been shown to remain unchanged (and probably under extreme functional constraint) over *H. sapiens* development (Pagano et al., 2021). The consistently small ratio of CET floor length to dilator tubae length among all but one of the *H. neanderthalensis* would be likely to result in marked differences in CET function during life, although the exact nature of this difference remains unclear. A clue may be found in the smaller values for this composite measure being most common among *H. sapiens* infants (as can be seen in the growth series) who exhibit the highest rates of otitis media as a result of their immature CET morphology

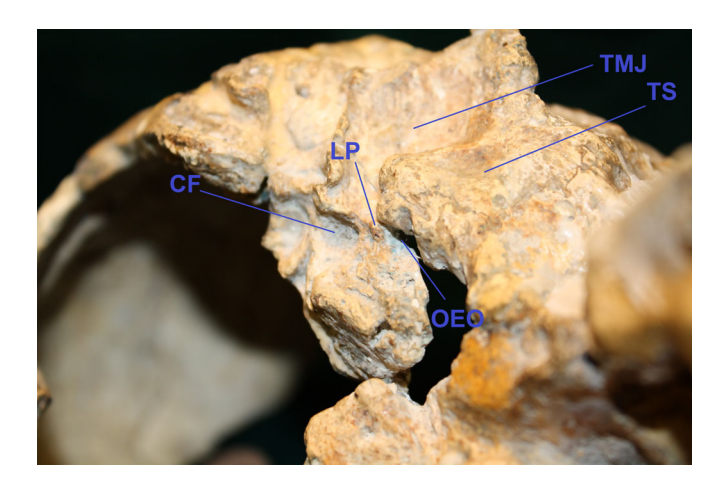


FIGURE 19 A basal view of the Forbes' Quarry 1 Neanderthal right-side temporal bone. Structures include temporomandibular joint surface (TMJ), temporal squama (TS), carotid foramen (CF), and osseous Eustachian tube orifice (OEO; plugged with matrix). Despite the levator process (LP) appearing more heavily eroded than in La Chapelle aux Saints 1 and Monte Circeo 1, its position is still observable

and function (Bluestone, 2005; Brooks, 1969; Jerger, 1970). We extrapolated previously (Pagano et al., 2019) that the H. neanderthalensis adult condition of horizontal CET orientation may have rendered children within those populations susceptible to otitis media for longer spans of their life histories, whereas vertical CET reorientation over H. sapiens development, associated with decreasing otitis media susceptibility (Bluestone, 2005), occurs around the same time that clinically observed rates of otitis media undergo steep decline (Kaur et al., 2017; Pagano et al., 2017, 2021; Paradise et al., 1997). The larger H. neanderthalensis sample in this study corroborates previous findings (Pagano et al., 2019) as this group exhibited the infant-like condition of more horizontal pterygoid plates relative to both the Frankfurt Horizontal Plane and the basicranium. Such an anatomical configuration would have led to less vertical space available for the torus tubarius and CET orifice on the lateral nasopharyngeal wall and an inferiorly lower placement of these structures that would approach the condition of contemporary H. sapiens infants. This condition also represents a marked morphological departure from both H. sapiens adults and from their common ancestor in the Middle Pleistocene as can be assessed from the mPH sample.

An additional consequence of the horizontal choanal orientation and anteroposteriorly elongated nasopharyngeal morphology of *H. neanderthalensis* is the potential for increased postnasal surface area, which could aid the nasal cavity in warming and humidifying inspiratory air. Anteroposteriorly elongated nasal cavities have been observed among *H. sapiens* populations from cold climates as a

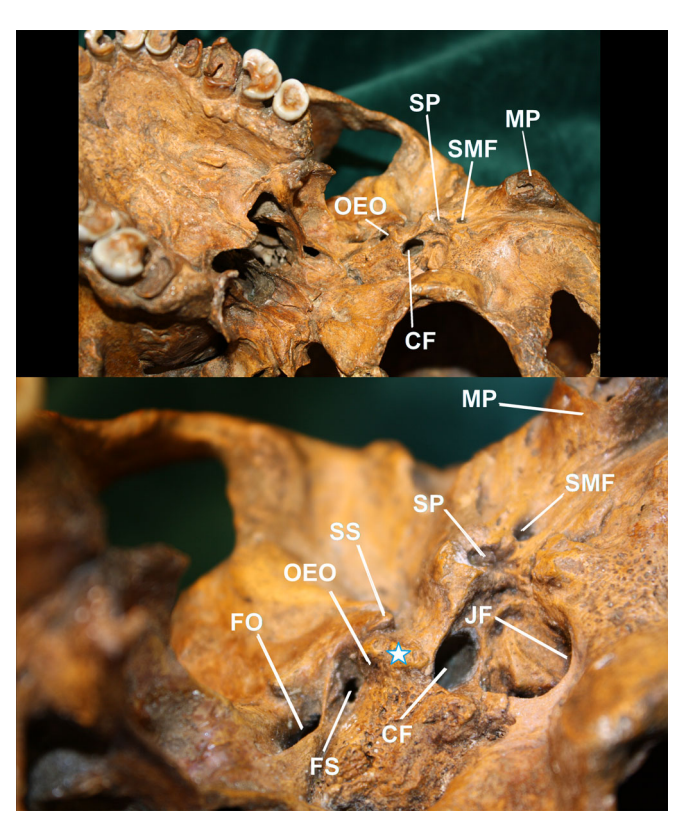
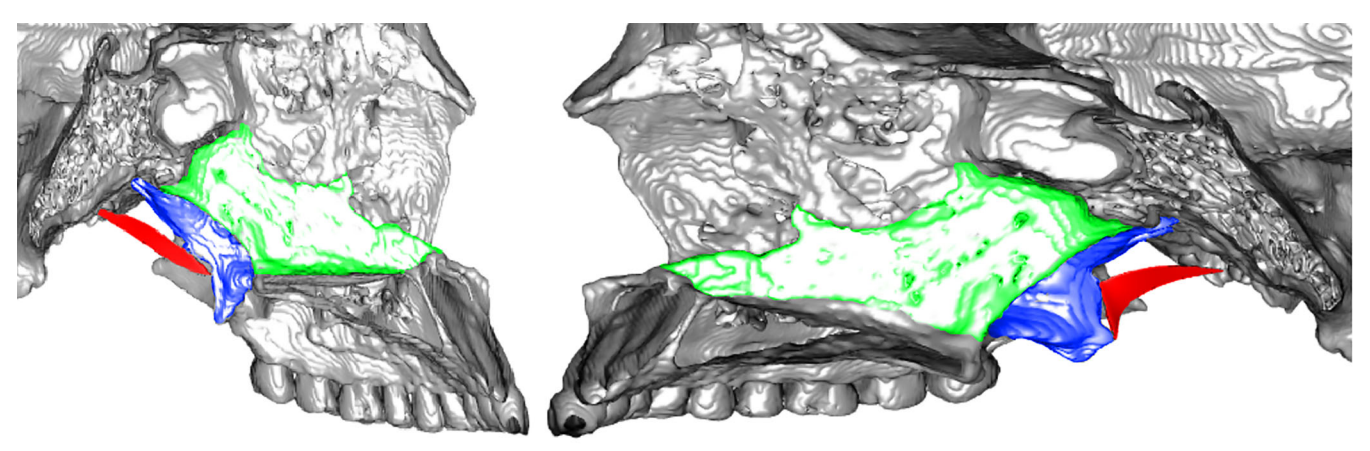


FIGURE 20 (Top) Basal view of the Kabwe 1 mid-Pleistocene cranium from Zambia. The relative positions of the osseous Eustachian tube orifice (OEO), carotid foramen (CF), base of the broken styloid process (SP), stylomastoid foramen (SMF), and mastoid process (MP) are all visible on the left side. Rotating this specimen to the right and viewing at higher magnification brings into focus the area surrounding the OEO. The sphenoid spine (SS) and foramen spinosum (FS) are visible but do not exhibit a modern human-like morphology as the foramen spinosum is not located in the spine. Also visible is the jugular foramen. Note that there is no levator process on this specimen, there being instead a ridge of bone (indicated by the star) between the osseous Eustachian tube orifice and carotid foramen resembling the modern human condition

means of increasing mucosal surface area (e.g., Evteev et al., 2014; Noback et al., 2011) and the continued elongation of the *H. neanderthalensis* postnasal airway may also achieve a similar functional outcome. Despite the primary role of the nasal cavity in warming and humidifying inspiratory airflow, subsequent warming and humidification occurs in the nasopharynx, oropharynx, and trachea, all of which contribute substantially to the conditioning of cold, dry ambient air before reaching the lungs (e.g., Naclerio et al., 2007; Perwitzschky, 1928). A medial projection of bone at the anterior nasal cavity of *H. neanderthalensis* (Laitman et al., 1996; Márquez et al., 2014; Schwartz & Tattersall, 1996; Schwartz et al., 2008) has been proposed to offer greater turbidity to inspiratory airflow and increased surface area for warming and humidifying cold, dry



Homo sapiens

Homo neanderthalensis

FIGURE 21 Warped mesh models of the average adult *Homo sapiens* and *Homo neanderthalensis*. The cartilaginous Eustachian tube is shaded red, the medial pterygoid plate and lateral nasal wall is shaded blue, and the vomer is shaded green. *H. sapiens* exhibit here a marked amount of basicranial flexion, anteroposterior shortening of the nasopharynx, vertical cartilaginous Eustachian (pharyngotympanic) tube (CET) orientation, and vertical vomeral orientation. *H. neanderthalensis* show instead an anteroposterior elongation of the nasopharynx, created in part by anterior rotation of the vomer and hard palate (i.e., more horizontal orientation), basicranial retroflexion, and horizontal orientation of the CET

ambient air. Recent computation fluid dynamics studies (Azevedo et al., 2017; Wroe et al., 2018) modeled airflow on a model of the H. neanderthalensis nasal cavity based, in part, on reconstructing missing aspects of H. neanderthalensis morphology from that of contemporary H. sapiens. They found that H. neanderthalensis exhibit some convergent evolution with cold-climate H. sapiens populations in increased nasal air conditioning capacity but that it was not as efficient as among contemporary high latitude H. sapiens. Relatively greater postnasal surface area could also assist a nasal cavity that, due to long, low cranial shape, may be functionally or biomechanically constrained from narrowing to the extent exhibited among cold-adapted H. sapiens populations (Márquez et al., 2014). More data are needed from 3D models and anatomical reconstruction of the postnasal airway to test this hypothesis.

5.3 | Nasopharyngeal morphology supports the accretionary hypothesis of Neanderthal origins

It remains unclear whether the *H. neanderthalensis* morphology of anteroposterior elongation and horizontal reorientation of the nasopharynx was the result of positive selection or stochastic factors. Multivariate and univariate analyses offer support to the accretionary hypothesis (Arsuaga et al., 1997) and our Hypothesis 1 as Atapuerca 5 and Steinheim 1 share the *H. neanderthalensis* pattern of horizontal choanal orientation (as measured by the orientation of the posterior vomeral

surface relative to the basisphenoid midline—the staphylion-hormion-sphenobasion angle and by the ratio of posterior vomeral edge length to medial pterygoid plate edge length). The GM analysis further shows that these two specimens were closer in overall nasopharyngeal morphology to Saccopastore 1, the geologically oldest H. neanderthalensis specimen in our sample, than were Petralona 1 and Kabwe 1. However, the Atapuerca 5 specimen appeared intermediate in position between the H. sapiens and H. neanderthalensis clusters, suggesting a less derived morphology. Thus, the metric data from Analysis 1 would support the exclusion of both Atapuerca 5 and Steinheim 1 from H. heidelbergensis (as redefined by Arsuaga et al., 2014) but the multivariate data from Analysis 2 indicate that Steinheim 1, the geologically oldest mPH specimen, is closer in overall nasopharyngeal morphology to the two H. erectus crania. The process of "neanderthalization" (Roksandic et al., 2018) appears to have happened in part via an accretionary process in the postnasal airway.

5.4 | The last common ancestor of *H. sapiens* and *H. neanderthalensis*

Both *H. sapiens* and *H. neanderthalensis* differ from mPH in possessing relatively shorter medial pterygoid plates, less vertically oriented CET morphology (relative to both the medial pterygoid plate posterior edge and to the Frankfort Horizontal Plane), and less vertically oriented dilator tubae muscles relative to the orientation of the common TVP tendon. It thus appears that the ancestral

condition for both *H. sapiens* and *H. neanderthalensis* includes extremely tall, vertically oriented choanae and more pronounced vertical orientation of the CET and dilator tubae as this condition is expressed in all the mPH crania. However, the medial pterygoid plates and CET floor of the two *H. erectus* specimens KNM-ER-3733 and Sangiran 17 are extremely horizontal as among *H. sapiens* infants. Thus, a two-step evolutionary pattern may have occurred as (1) the more vertical medial pterygoid plates and CETs of mPH emerged from the horizontal morphology of *H. erectus* and (2) the common ancestor of *H. sapiens* and *H. neanderthalensis* diverged by becoming relatively more horizontal.

H. erectus crania exhibit extremely tall and narrow choanae and an extremely narrow basicranium relative to all other specimens, as is found among nonhuman hominoids (Pagano & Laitman, 2015). The common ancestor of H. sapiens and H. neanderthalensis likely exhibited a new morphological pattern relative to its presumed ancestor, H. erectus, in mediolateral broadening and vertical shortening of the postnasal airway but, subsequently, each group underwent opposite patterns of change with H. neanderthalensis increasing the anteroposterior length of their postnasal airways while those of H. sapiens became anteroposteriorly shorter as a result of marked orthognathy and basicranial flexion (Figure 21). H. sapiens and H. neanderthalensis thus appear to each exhibit autapomorphies in the osseous nasopharyngeal boundaries and CET apparatus relative to each other and to H. erectus (Figure 22). H. sapiens further exhibits extreme vertical orientation of medial pterygoid plates relative to the Frankfort Horizontal Plane and the most mediolaterally broad and vertically short airway of any group. Based metric and GM analysis, H. neanderthalensis possessed horizontal choanal orientation, relative elongation of the dilator tubae muscle, and retroflexion of the cranial base between hormion and endobasion. H. neanderthalensis occupied the extreme range of H. sapiens variation in exhibiting airorhynch facial morphology, horizontal orientation of the medial pterygoid plates relative to the Frankfort Horizontal Plane (a measure of CET orientation related to the position of its lateral lamina), greater relative dilator tubae length, and a more acute angle at which the CET floor meets the medial pterygoid plate posterior edge (a function of the horizontal orientation of the latter).

Petralona 1 and Kabwe 1 are nested among *H. sapiens* in the PCA and differ from *H. sapiens* adults only in those univariate measures related generally to cranial robusticity (supporting Hypothesis 2). The morphological similarity of these two specimens has been noted previously (Freidline et al., 2012; Friess, 2010; Harvati, 2009; Harvati et al., 2010, 2011; Murrill, 1981; Rightmire, 2001;

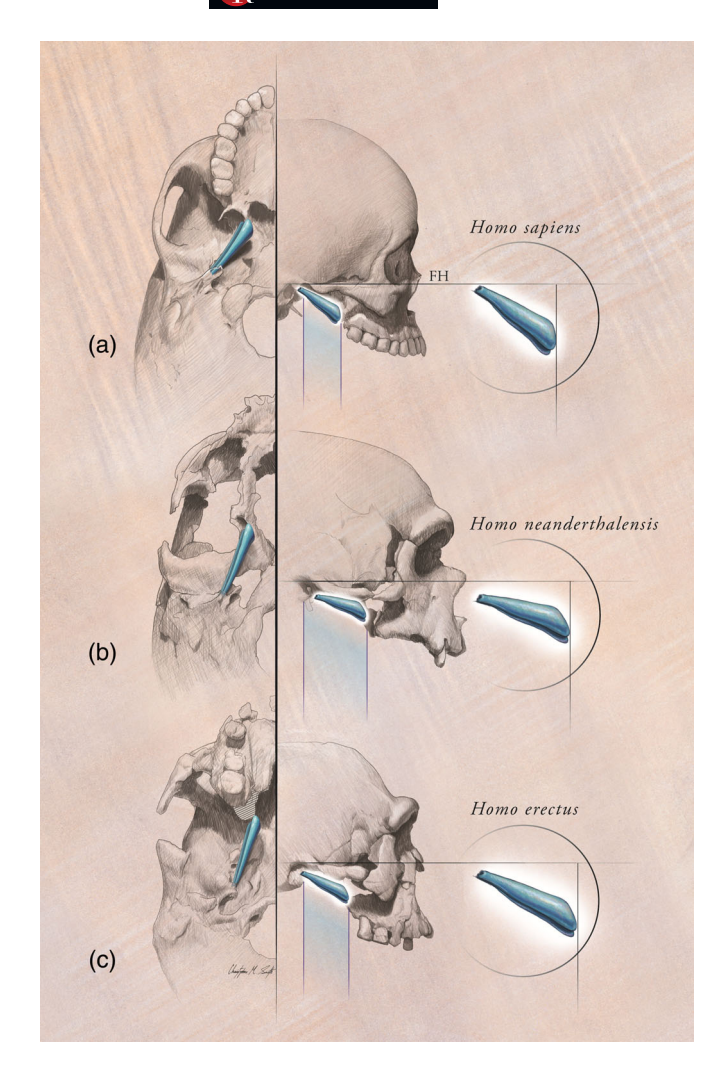


FIGURE 22 A visual comparison of nasopharyngeal and cartilaginous Eustachian (pharyngotympanic) tube (CET) morphology among (a) *Homo sapiens*, (b) *Homo neanderthalensis*, and (c) *Homo erectus*. Left side: basicranial view; right side: right lateral view. Anteroposterior dimensions of nasopharynx are highlighted in blue. Gray shaded area in "C" denotes reconstructed bone. *H. sapiens* is distinguished in having more vertical CET orientation and an anteroposteriorly short nasopharynx whereas *H. neanderthalensis* exhibits the opposite pattern of an anteroposteriorly elongated nasopharynx and a horizontally oriented CET. *H. erectus* has a relatively long CET that is oriented more medially due to tall, narrow choanae

Seidler et al., 1997; Stringer, 1983; Stringer et al., 1979) and is corroborated here. The lack of *H. neanderthalensis* morphology in Petralona 1 both in Analyses 1 and 2 supports the conclusions of Roksandic et al. (2018) that mid-Pleistocene hominins in the Eastern Mediterranean were connected by geneflow to other regions of Western Asia and Africa, maintaining plesiomorphic morphology (or ancestral morphology that arose early in the lineage of mPH). Of equal note is the position of KNM-ER 3733 and Sangiran 17 on the PCA plots of Analysis 2. These two

crania are more robust (i.e., tall and narrow) in overall postnasal morphology and likely more ancestral relative to the
respective conditions of the *H. sapiens* and *H. neanderthalensis*. Analysis 1 confirms that both specimens exhibit aspects of their morphology outside both *H. sapiens* and *H. neanderthalensis* ranges of variation,
likely representing the ancestral state from which they originated but diverged subsequently. Hypothesis 3 is thus
supported.

6 | CONCLUSIONS

While some aspects of basicranial morphology have been used in phylogenetic analyses (e.g., Ahern, 1998; Harvati, 2003; Rightmire et al., 2017), the osseous nasopharyngeal boundaries, CET, and dilator tubae have rarely been considered as a source of characters. Yet, this system serves several vital functions including assistance in swallowing, resonation for speech sounds, and ventilation of the middle ear. Evolutionary changes within nasopharyngeal structures have had a pronounced impact on the fitness of our species and may provide a novel perspective on the origins of *H. sapiens* and *H. neanderthalensis*. As more evidence is brought to bear, the mid-Pleistocene fossil record becomes less muddled but increasingly complex.

AUTHOR CONTRIBUTIONS

Anthony S. Pagano: Writing – original draft (equal). Christopher M. Smith: Writing – original draft (equal). Antoine Balzeau: Writing – original draft (equal). Samuel Márquez: Writing – original draft (equal). Jeffrey T. Laitman: Writing – original draft (equal). This manuscript is a contribution to the NYCEP Morphometrics group (NMG 117).

ORCID

Anthony S. Pagano https://orcid.org/0000-0002-2323-5561

Christopher M. Smith https://orcid.org/0000-0001-9259-1079

Antoine Balzeau https://orcid.org/0000-0002-4226-611X

Samuel Márquez https://orcid.org/0000-0002-9764-1597

Jeffrey T. Laitman https://orcid.org/0000-0002-9629-946X

REFERENCES

Adams, D., Collyer, M., Kaliontzopoulou, A., Baken, E. (2021). Geomorph: Software for geometric morphometric analyses. R package version 4.0. https://cran.r-project.org/package=geomorph

- Ahern, J. C. M. (1998). Underestimating intraspecific variation: The problem with excluding Sts 19 from *Australopithecus africanus*. *American Journal of Physical Anthropology*, 105, 461–480.
- Anton, S. C. (2003). Natural history of *Homo erectus*. Yearbook of *Physical Anthropology*, 46, 126–170.
- Arsuaga, J. L., Martinez, I., Gracia, A., & Lorenzo, C. (1997). The Sima de los Huesos crania (Sierra de Atapuerca, Spain). A comparative study. *Journal of Human Evolution*, *33*, 219–281.
- Arsuaga, J. L., Martínez, I., Arnold, L. J., Aranburu, A., Gracia-Téllez, A., Sharp, W. D., Quam, R. M., Falguères, C., Pantoja-Pérez, A., Bischoff, J., Poza-Rey, E., Parés, J. M., Carretero, J. M., Demuro, M., Lorenzo, C., Sala, N., Martinon-Torres, M., Garcia, N., Alcazar de Velasco, A., ... Carbonell, E. (2014). Neandertal roots: Cranial and chronological evidence from Sima de los Huesos. *Science*, 344, 1358–1363.
- Ashton, E. H. (1957). Age changes in the basicranial axis of the Anthropoidea. Proceedings of the Zoological Society of London, 129, 5–74.
- Athreya, S. (2007). Was *Homo heidelbergensis* in South Asia? A test using the Narmada fossil from Central India. In M. D. Petraglia & B. Allchin (Eds.), *The evolution and history of human populations in South Asia* (pp. 137–170). Springer.
- Avery, D. M. (2002). Taphonomy of micromammals from cave deposits at Kabwe (Broken Hill) and twin Rivers in Central Zambia. *Journal of Archaeological Science*, 29, 537–544.
- Azevedo, S., González, M. F., Cintas, C., Ramallo, V., Quinto-Sánchez, M., Márquez, F., Hünemeier, T., Paschetta, C., Ruderman, A., Navarro, P., Pazos, B. A., Silva de Cerqueira, C. C., Velan, O., Ramírez-Rozzi, F., Calvo, N., Castro, H. G., Paz, R. R., & Gonzalez-Jose, R. (2017). Nasal airflow simulations suggest convergent adaptation in Neanderthals and modern humans. *Proceedings of the National Academy of Sciences*, 114, 12442–12447.
- Baab, K. L. (2008). The taxonomic implications of cranial shape variation in Homo erectus. *Journal of Human Evolution*, *54*, 827–847.
- Barham, L. S., & Smart, P. L. (1996). An early date for the middle stone age of Central Zambia. *Journal of Human Evolution*, 30, 287–290.
- Bastir, M. (2019). Big choanae, larger face: Scaling patterns between cranial airways in modern humans and African apes and their significance in middle and late Pleistocene hominin facial evolution. Bulletins et Mémoires de la Société d'Anthropologie de Paris, 31, 5–13.
- Bastir, M., & Rosas, A. (2016). Cranial base topology and basic trends in the facial evolution of *Homo. Journal of Human Evolution*, 91, 26–35.
- Bermúdez de Castro, J. M., Martinón-Torres, M., Martínez de Pinillos, M., García-Campos, C., Modesto-Mata, M., Martín-Frances, L., & Arsuaga, J. L. (2019). Metric and morphological comparison between the Arago (France) and Atapuerca-Sima de los Huesos (Spain) dental samples, and the origin of Neanderthals. *Quaternary Science Reviews*, 217, 45–61.
- Bischoff, J., Williams, R. W., Rosenbauer, R. J., Aramburu, A., Arsuaga, J. L., Garcia, N., & Cuenca-Bescos, G. (2007). High-resolution U-series dates from the Sima de los Huesos hominids yields 600^{+∞}₋₆₆ kyrs: Implications for the evolution of the early Neanderthal lineage. *Journal of Archaeological Science*, 34, 763–770.

- Bluestone, C. D. (2005). The Eustachian tube: Structure, function, role in otitis media. BC Decker.
- Bluestone, C. D., Pagano, A. S., Swarts, J. D., & Laitman, J. T. (2012). Consequences of evolution: Is rhinosinusitis, like otitis media, a unique disease of humans? *Otolaryngology—Head and Neck Surgery*, 147(6), 986–991.
- Bolter, D. R., & Zihlman, A. L. (2003). Morphometric analysis of growth and development in wild-collected vervet monkeys (*Cercopithecus aethiops*), with implications for growth patterns in Old World monkeys, apes and humans. *Journal of Zoology*, 260, 99–110.
- Bräuer, G. (2008). The origin of modern anatomy: By speciation or intraspecific evolution. *Evolutionary Anthropology*, 17, 22–37.
- Brooks, D. (1969). The use of the electro-acoustic impedance bridge in the assessment of middle ear pressures. *International Audiology*, *8*, 563–569.
- Cave, A. J. E. (1979). The mammalian tempro-pterygoid ligament. *Journal of Zoology*, 188, 517–532.
- Cooke, S. B., & Terhune, C. E. (2015). Form, function, and geometric morphometrics. *The Anatomical Record*, 298, 5–28.
- Day, M. H. (1969). Early *Homo sapiens* remains from the Omo River region of Southwest Ethiopia. *Nature*, *222*, 1132–1138.
- Dean, M. C. (1982). The comparative myology of the hominoid cranial base [PhD Dissertation, The Middlesex Hospital Medical School, University of London].
- Dean, D., Hublin, J.-J., Holloway, R., & Ziegler, R. (1998). On the phylogenetic position of the pre-Neanderthal specimen from Reilingen, Germany. *Journal of Human Evolution*, 34, 485–508.
- Dean, M. C., & Wood, B. A. (1982). Basicranial anatomy of Plio-Pleistocene hominids from east and South Africa. *American Journal of Physical Anthropology*, 59, 157–174.
- Dechant, D. (2000). Skeletons in the closet: The Spencer R. Atkinson library of applied anatomy. *Contact Point*, 80(3), 15–19
- Delson, E., Harvati, K., Reddy, D., Marcus, L. F., Mowbray, K., Sawyer, G. J., Jacob, T., & Marqeuz, S. (2001). Sambungmacan 3 Homo erectus calvaria: A comparative morphometric and morphological analysis. The Anatomical Record, 262, 380–397.
- Demuro, M., Arnold, L. J., Aranburu, A., Sala, N., & Arsuaga, J.-L. (2019). New bracketing luminescence ages constrain the Sima de los Huesos hominin fossils (Atapuerca, Spain) to MIS 12. *Journal of Human Evolution*, 131, 76–96.
- De Quieroz, K., & Gauthier, J. A. (1992). Phylogenetic taxonomy. Annual Review of Ecology and Systematics, 23, 449–480.
- Doyle, W. J., & Rood, S. R. (1979). Anatomy of the auditory tube and related structures in the rhesus monkey (*Macaca mulatta*). *Acta Anatomica*, 105, 209–225.
- Doyle, W. J., & Rood, S. R. (1980). Comparison of the anatomy of the Eustachian tube in the rhesus monkey (*Macaca mulatta*) and man: Implications for physiologic modeling. *Annals of Otology, Rhinology & Laryngology*, 89, 49–57.
- Evteev, A., Cardini, A. L., Morozova, I., & O'Higgins, P. (2014).
 Extreme climate, rather than population history, explains midfacial morphology of northern Asians. American Journal of Physical Anthropology, 153, 449–462.
- Freidline, S. E., Gunz, P., Harvati, K., & Hublin, J. J. (2012). Middle Pleistocene human facial morphology in an evolutionary and developmental context. *Journal of Human Evolution*, *63*, 723–740.

- Friess, M. (2010). Calvarial shape variation among Middle Pleistocene hominins: An application of surface scanning in paleoanthropology. *Comptes Rendus Palevol*, *9*, 435–443.
- Grün, R., & Stringer, C. B. (1991). ESR dating and the evolution of modern humans. *Archaeometry*, *33*, 153–199.
- Grün, R. (1996). A re-analysis of electron spin resonance dating results associated with the Petralona hominid. *Journal of Human Evolution*, 30(3), 227–241.
- Grün, R., Pike, A., McDermott, F., Eggins, S., Mortimer, G., Aubert, M., Kinsley, L., Joannes-Boyau, R., Rumsey, M., Denys, C., Brink, J., Clark, T., & Stringer, C. (2020). Dating the skull from Broken Hill, Zambia, and its position in human evolution. *Nature*, 580, 372–375.
- Gunz, P., Mitteroecker, P., Neubauer, S., Weber, G. W., & Bookstein, F. L. (2009). Principles for the virtual reconstruction of hominin crania. *Journal of Human Evolution*, 57, 48–62.
- Hanegraef, H., Martinón-Torres, M., Martínez de Pinillos, M., Martín-Francés, L., Vialet, A., Arsuaga, J. L., & María Bermúdez de Castro, J. (2018). Dentine morphology of Atapuerca-Sima de los Huesos lower molars: Evolutionary implications through three-dimensional geometric morphometric analysis. American Journal of Physical Anthropology, 166, 276–295.
- Harvati, K. (2003). The Neanderthal taxonomic position: Models of intra- and inter-specific craniofacial variation. *Journal of Human Evolution*, 44, 107–132.
- Harvati, K. (2009). Petralona: Link between Africa and Europe? In L. Schepartz, C. Bourbou, & S. Fox (Eds.), New directions in the skeletal biology of Greece Wiener Laboratory Series (pp. 31–47). ASCSA
- Harvati, K., Hublin, J. J., & Gunz, P. (2010). Evolution of middlelate Pleistocene human cranio-facial form: A 3-D approach. *Journal of Human Evolution*, 59, 445–464.
- Harvati, K., Stringer, C., Grün, R., Aubert, M., Allsworth-Jones, P., & Folorunso, C. A. (2011). The later stone age calvaria from Iwo Eleru, Nigeria: Morphology and chronology. *PLoS One*, 6, e24024.
- Hellman, M. (1927). Changes in the human face brought about by development. *International Journal of Orthodontia*, *Oral Surgery and Radiography*, 13, 475–515.
- Hennig, W. (1966). In D. D. Davis & R. Zangerl(Trans.), *Phylogenetic systematics*. University of Illinois Press.
- Hofer, H. (1952). Der Gestaltwandel des Schädels der Säugetiere und Vögel mit besonderer Berücksichtigung der Knickungstypen und der Schädelbasis. *Verhandlungen der Anatomischen Gesellschaft*, 50, 102–113.
- Howells, W. W. (1980). *Homo erectus*—Who, when, and where: A survey. *Yearbook of Physical Anthropology*, 23, 1–23.
- Huang, M. H., Lee, S. T., & Rajendran, K. (1997). Anatomic basis of cleft palate and velopharyngeal surgery: Implications from a fresh cadaveric study. *Plastic and Reconstructive Surgery*, 101, 833–842.
- Hublin, J.-J. (2009). The origin of Neandertals. *Proceedings of the National Academy of Sciences*, 106, 16022–16027.
- Hublin, J.-J., Ben-Ncer, A., Bailey, S. E., Freidline, S. E., Neubauer, S., Skinner, M. M., Bergmann, I., Le Cabec, A., Benazzi, S., Harvati, K., & Gunz, P. (2017). New fossils from Jebel Irhoud, Morocco and the pan-African origin of *Homo sapiens*. Nature, 546, 289–292.

- Isaac, G. L. L. (1975). Sorting out the muddle in the middle: An anthropologist's post-conference appraisal. In K. Butzer & G. L. L. Isaac (Eds.), After the australopithecines: Stratigraphy, ecology, and cultural change in the Middle Pleistocene (pp. 875–888). Mouton Publishers.
- Jerger, J. (1970). Clinical experiences with impedance audiometry. *Archives of Otolaryngology*, 92, 311–324.
- Kaur, R., Morris, M., & Pichichero, M. E. (2017). Epidemiology of acute otitis media in the postpneumococcal conjugate vaccine era. *Pediatrics*, 140, e20170181.
- Laitman, J. T., Heimbuch, R. C., & Crelin, E. S. (1979). The basicranium of fossil hominids as an indicator of their upper respiratory systems. *American Journal of Physical Anthropology*, 51, 15–34.
- Laitman, J. T., & Heimbuch, R. C. (1982). The basicranium of Plio-Pleistocene hominids as an indicator of their upper respiratory tract. *American Journal of Physical Anthropology*, 59, 323–343.
- Laitman, J. T., Reidenberg, J. S., Marquez, S., & Gannon, P. J. (1996).
 What the nose knows: New understandings of Neanderthal upper respiratory tract specializations. Proceedings of the National Academy of Sciences of the United States of America, 93, 10543–10545.
- Laitman, J. T., & Reidenberg, J. S. (2009). The evolution of the human larynx: nature's great experiment. In M. P. Fried & A. Ferlito (Eds.), *The larynx, Volume Three* (pp. 19–38). San Diego: Plural.
- Lepre, C. J., & Kent, D. V. (2015). Chronostratigraphy of KNM-ER 3733 and other Area 104 hominins from Koobi Fora. *Journal of Human Evolution*, 86, 99–111.
- Maier, N., & Nkini, A. (1984). Olduvai hominid 9: New results of investigation. In P. Andrews & J. L. Franzen (Eds.), *The early* evolution of man (Vol. 69, pp. 69–82). Cour Forsch Inst Senckenberg.
- Márquez, S., Pagano, A. S., Delson, E., Lawson, W., & Laitman, J. T. (2014). The nasal complex of Neanderthals: An entry portal to their place in human ancestry. *The Anatomical Record*, 297, 2121–2137.
- Martinón-Torres, M., de Castro, J. M. B., Gomez-Robles, A., Prado-Simon, L., & Arsuaga, J. L. (2012). Morphological description and comparison of the dental remains from Atapuerca-Sima de los Huesos site (Spain). *Journal of Human Evolution*, 62, 7–58.
- Martinón-Torres, M., & Bermúdez de Castro, J. M. (2015). The hominins 2:The genus *Homo*. In J. D. Irish & R. G. Scott (Eds.), *A* companion to dental anthropology (pp. 67–84). John Wiley & Sons, Inc..
- Mayr, E. (1950). Taxonomic categories in fossil hominids. Cold Spring Harbor Symposia on Quantitative Biology. The Biological Laboratory, Cold Spring Harbor, New York, pp. 109–118.
- Mounier, A., & Lahr, M. M. (2016). Virtual ancestor reconstruction: Revealing the ancestor of modern humans and Neandertals. *Journal of Human Evolution*, 91, 57–72.
- Murrill, R. I. (1981). Petralona man: A new description and comparative study, with new information on Rhodesian man. Charles Thomas
- Naclerio, R. M., Pinto, J., Assanasen, P., & Baroody, F. M. (2007). Observations on the nose to warm and humidify inspired air. *Rhinology*, 45, 102–111.
- Negus, V. E. (1949). The comparative anatomy and physiology of the larynx. W.n. Heinemann.

- Noback, M. L., Harvati, K., & Spoor, F. (2011). Climate-related variation of the human nasal cavity. American Journal of Physical Anthropology, 145, 599–614.
- Pagano, A. S. (2014). The development and function of the nasopharynx and its role in the evolution of primate respiratory abilities [PhD Dissertation, City University of New York Graduate Center].
- Pagano, A. S., & Laitman, J. T. (2015). Three-dimensional geometric morphometric analysis of the nasopharyngeal boundaries and its functional integration with the face and external basicranium among extant hominoids. *The Anatomical Record*, 298, 85–106.
- Pagano, A. S., Wang, E., Yuan, D., Fischer, D., Bluestone, C. D., Marquez, S., & Laitman, J. T. (2017). Cranial indicators identified for peak incidence of otitis media. *The Anatomical Record*, 300, 1721–1740.
- Pagano, A. S., Marquez, S., & Laitman, J. T. (2019). Reconstructing the Neanderthal Eustachian tube: New insights on disease susceptibility, fitness cost, and extinction. *The Anatomical Record*, 302, 2109–2125.
- Pagano, A. S., Márquez, S., Smith, C. M., & Laitman, J. T. (2021). Identification of critical windows in early development of human upper respiratory tract and middle ear disease. *The Anatomical Record*, 304, 1953–1973. https://doi.org/10.1002/ar. 24600
- Paradise, J. L., Rockette, H. E., Colborn, D. K., Bernard, B. S., Smith, C. G., Kurs-Lasky, M., & Janoski, J. E. (1997). Otitis media in 2253 Pittsburgh-area infants: Prevalence and risk factors during the first two years of life. *Pediatrics*, 99, 318–333.
- Perwitzschky, R. (1928). Die temperature und feuchtigkeitsverhaltnisse der atemluft in den luftwegen. *Arch Ohren- Nasen- Kehlkkopfheilkunde*, 117(1), 1–136.
- Rendu, W., Beauval, C., Crevecoeur, I., Bayle, P., Balzeau, A., Bismuth, T., Bourguignon, L., Delfour, G., Faivre, J.-P., Lacrampe-Cuyaubère, F., Tavormina, C., Todisco, D., Turq, A., & Maureille, B. (2014). Evidence supporting an intentional Neandertal burial at La Chapelle-aux-saints. Proceedings of the National Academy of Sciences, 111, 81–86.
- Rightmire, P. G. (1990). The evolution of Homo erectus; comparative anatomical studies of an extinct human species. Cambridge University Press.
- Rightmire, G. P. (1998). Human evolution in the Middle Pleistocene: The role of Homo heidelbergensis. Evolutionary Anthropology, 6, 218–227.
- Rightmire, G. P. (2001). Patterns of hominid evolution and dispersal in the Middle Pleistocene. *Quaternary International*, *75*, 77–84.
- Rightmire, G. P., Lorkipanidze, D., & Vekua, A. (2006). Anatomical descriptions, comparative studies and evolutionary significance of the hominin skulls from Dmanisi, Republic of Georgia. *Jour*nal of Human Evolution, 50, 115–141.
- Rightmire, G. P., Ponce de León, M. S., Lordkipanidze, D., Margvelashvili, A., & Zollikofer, C. P. E. (2017). Skull 5 from Dmanisi: Descriptive anatomy, comparative studies, and evolutionary significance. *Journal of Human Evolution*, 104, 50–79.
- Rohan, R. F., & Turner, L. (1956). The levator palati muscle. *Journal of Anatomy*, 90, 153–154.
- Roksandic, M., Radovic, P., & Lindal, J. (2018). Revising the hypodigm of *Homo heidelbergensis*: A view from the eastern Mediterranean. *Quaternary International*, 466, 66–81.

- Ross, C. F., & Ravosa, M. J. (1993). Basicranial flexion, relative brain size, and facial kyphosis in nonhuman primates. *Ameri*can *Journal of Physical Anthropology*, 91, 305–324.
- Santa Luca, A. (1978). A re-examination of presumed Neandertallike fossils. *Journal of Human Evolution*, 7, 619–636.
- Schoetensack, O. (1908). Der unterkiefer des Homo heidelbergensis aus den Sanden von Mauer bei Heidelberg. Ein Beitrag zur Palaontologie des Menschen. Wilhelm Engelmann.
- Schwarcz, H. P., Bietti, A., Buhay, W. M., Stiner, M. C., Grun, R., & Segre, A. (1991). On the reexamination of Grotta Guattari: Uranium-series and electron-spin-resonance dates. *Current Anthropology*, *32*, 313–316.
- Schwartz, J. H., & Tattersall, I. (1996). Significance of some previously unrecognized apomorphies in the nasal region of Homo neanderthalensis. *Proceedings of the National Academy of Sciences USA*, 93, 10852–10854.
- Schwartz, J. H., Tattersall, I., & Teschler-Nicola, M. (2008). Architecture of the nasal complex in Neanderthals: Comparison with other hominids and phylogenetic significance. *The Anatomical Record*, 291, 1517–1534.
- Seidler, H., Falk, D., Stringer, C., Wilfing, H., Müller, G. B., zur Nedden, D., Weber, G. W., Reicheis, W., & Arsuaga, J. L. (1997). A comparative study of stereolithographically modelled skulls of Petralona and Broken Hill: Implications for future studies of Middle Pleistocene hominid evolution. *Journal of Human Evolution*, 33, 691–703.
- Shen, G., & Yokoyama, Y. (1984). Th-230/U-234 dating of Petralona speleothems. *Anthropos*, 11, 23–32.
- Sherratt, E. (2015). Quick Guide to Geomorph v.2.1.6. https://www.researchgate.net/file.PostFileLoader.html?id= 57e24b67f7b67eef2604c789&assetKey=AS% 3A408679657558016%401474448231372
- Skinner, M. M., de Vries, D., Gunz, P., Kupczik, K., Klassen, R. P., Hublin, J. J., & Roksandic, M. (2016). A dental perspective on the taxonomic affinity of the Balanica mandible (BH-1). *Journal of Human Evolution*, *93*, 63–81.
- Spoor, F. (1997). Basicranial architecture and relative brain size of Sts 5 (Australopithecus africanus) and other Plio-Pleistocence hominids. South African Journal of Science, 93, 182–186.
- Starck, D. (1953). Morphologische Untersuchungen am Kopf der Säugetiere, besonders der Prosimier, ein Beitrag zum Problem des Formwandels des Säugetierschädels. Zeitschrift für Wissenschaftliche Zoologie, 157, 169–219.
- Stratovan Corporation. (2021). Stratovan Checkpoint [Software].

 Version x64. https://www.stratovan.com/products/checkpoint
- Stringer, C. B., Howell, F. C., & Melentis, J. K. (1979). The significance of the fossil hominid skull from Petralona, Greece. *Journal of Archaeological Science*, 6, 235–253.
- Stringer, C. B. (1983). Some further notes on the morphology and dating of the Petralona hominid. *Journal of Human Evolution*, 12, 731–742.
- Stringer, C. B. (2012). The status of *Homo heidelbergensis* (Schoetensack 1908). *Evolutionary Anthropology: Issues, News, and Reviews, 21,* 101–107.

- Takagi, Y., Waters, J., & Bosma, J. (1962). Anatomical studies of the epipharyngeal walls in relation to the base of the cranium. *Annals of Otology, Rhinology and Laryngology*, 71, 366–376.
- Talamo, S., Aldeias, V., Goldberg, P., Chiotti, L., Dibble, H. L., Guefin, G., Hublin, J.-J., Madelaine, M. R., Sandgathe, D., Steele, T. E., Turq, A., & McPherron, S. J. P. (2020). The new ¹⁴C chronology for the Paleolithic site of La Ferrasie, France: The disappearance of Neanderthals and the arrival of *Homo sapiens* in France. *Journal of Ouaternary Science*, 35(7), 961–973.
- Tattersall, I. (1986). Species recognition in human paleontology. *Journal of Human Evolution*, 15, 165–175.
- Tattersall, I., & Schwartz, J. H. (1998). Morphology, paleoanthropology, and Neanderthals. The Anatomical Record, 253, 113–117.
- Wagner, G. A., Krbetschek, M., Degering, D., Bahain, J.-J., Shao, Q., Falgueres, C., Voinchet, P., Dolo, J.-M., Garcia, T., & Rightmire, G. P. (2010). Radiometric dating of the type-site for Homo heidelbergensis at Mauer, Germany. Proceedings of the National Academy of Sciences, 107, 19726–19730.
- Wang, S. L. (2011). Regional isolation and extinction? The story of the mid-Pleistocene hominins in Asia (abstract). American Journal of Physical Anthropology, 50, s304–s305.
- Weidenreich, F. (1943). The skull of Sinanthropus pekinensis: A comparative study on a primitive hominid skull. Geological Survey of China.
- Weidenreich, F. (1951). Morphology of Solo man. Anthropological Papers of the American Museum of Natural History, 43, 222–288.
- White, T. D., Asfaw, B., DeGusta, D., Gilbert, H., Richards, G. D., Suwa, G., & Clark, H. F. (2003). Pleistocene *Homo sapiens* from middle awash, Ethiopia. *Nature*, *423*, 742–747.
- Wroe, S., Parr, W. C. H., Ledogar, J. A., Bourke, J., Evans, S. P., Florenza, L., Benazzi, S., Hublin, J.-J., Stringer, C., Kullmer, O., Curry, M., Rae, T. C., & Yokley, T. R. (2018). Computer simulations show that Neanderthal facial morphology represents adaptation to cold and high energy demands, but not heavy biting. *Proceedings of the Royal Society B*, 285, 20180085.
- Xiao, D., Bae, C. J., Shen, G., Delson, E., Jin, J. H. J., Webb, N. M., & Qiu, L. (2014). Metric and geometric morphometric analysis of new hominin fossils from Maba (Guandong, China). *Journal of Human Evolution*, 74, 1–20.
- Zaim, Y., Ciochon, R. L., Polanski, J. M., Grine, F. E., Bettis, E. A., III, Rizal, Y., Franciscus, R. G., Larick, R. R., Heizler, M., Aswan, E. K. L., & Marsh, H. E. (2011). New 1.5 million-yearold *Homo erectus* maxilla from Sangiran (Central Java, Indonesia). *Journal of Human Evolution*, 61, 363–376.

How to cite this article: Pagano, A. S., Smith, C. M., Balzeau, A., Márquez, S., & Laitman, J. T. (2022). Nasopharyngeal morphology contributes to understanding the "muddle in the middle" of the Pleistocene hominin fossil record. *The Anatomical Record*, 1–27. https://doi.org/10.1002/ar.24913